APPENDIX 2 SOIL TESTS AROUND THE EXTENDED BREAKWATER

During the finalization of the Second Stage Expansion Project Plan for the Port of Caldera, boreholes were drilled and soil tests performed along the center line of the breakwater extension, and the results thereof are shown in Fig. M－1～M－4. The locations of the boreholes are shown in CHAPTER IV, 4. Soil Conditions, Fig. IV－16.

Listed in the results of the soil tests are columnar soil compostion charts, sampling depth, N value from the standard penetration test, sand-silt-clay percentage composition, unit weight, specific weight of soil particles, natural moisture content, liquid limit, plastic limit, void ratio, compression index, unconfined compression strength, consolidation yield stress, and internal friction angle and cohesion according to unconsolidated undrained triaxial compression test results.

Boring was carried out by the wash method, and the sea scaffolding made use of a tower constructed of steel tubing with attached floats. Sampling for soil tests was carried out using a BX Shelby tube (open sampler of 50 mm diameter).

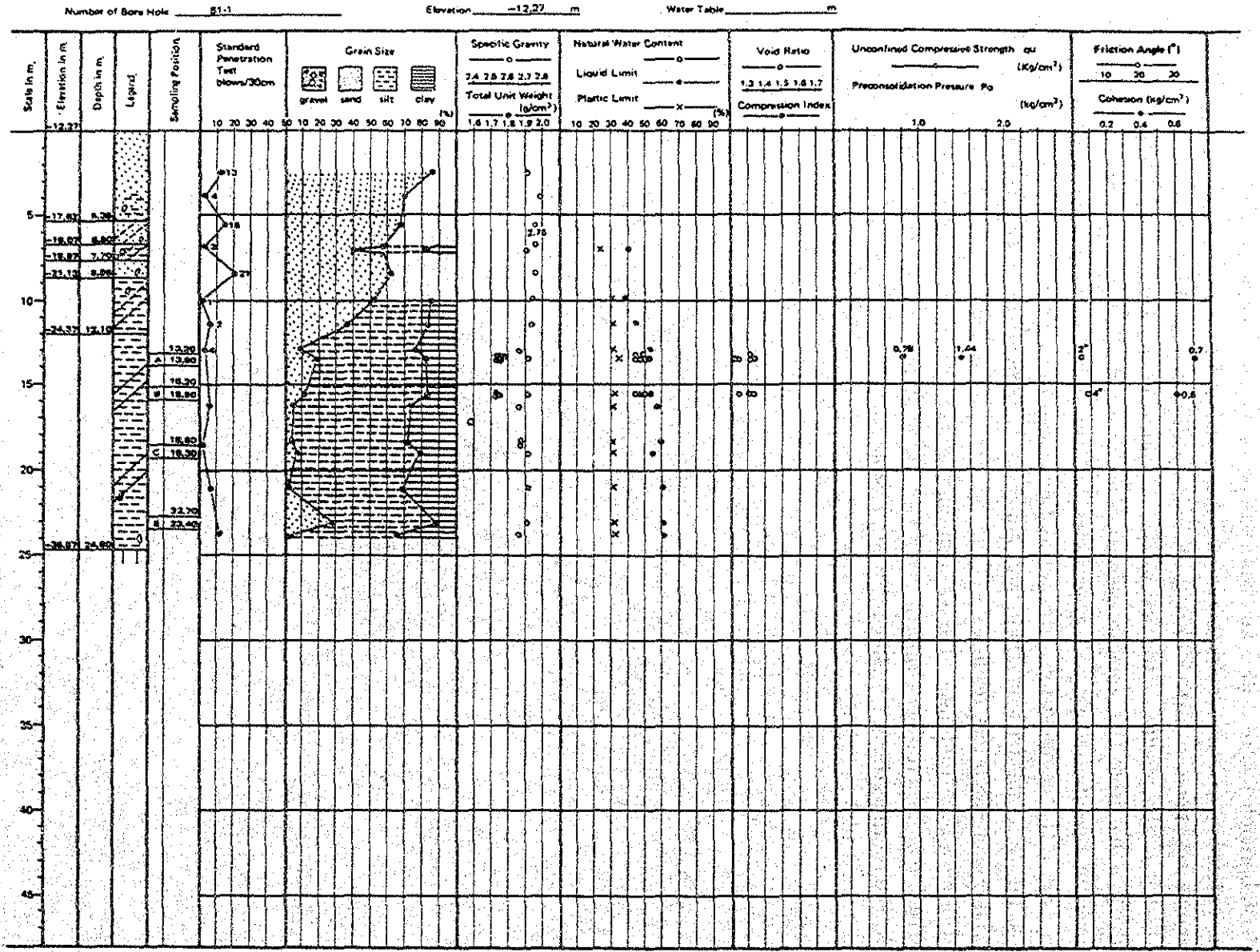

Fig. M-1 Summary of Results of Soil Tests around the Extended Breakwater (Borehole No. 81-1)

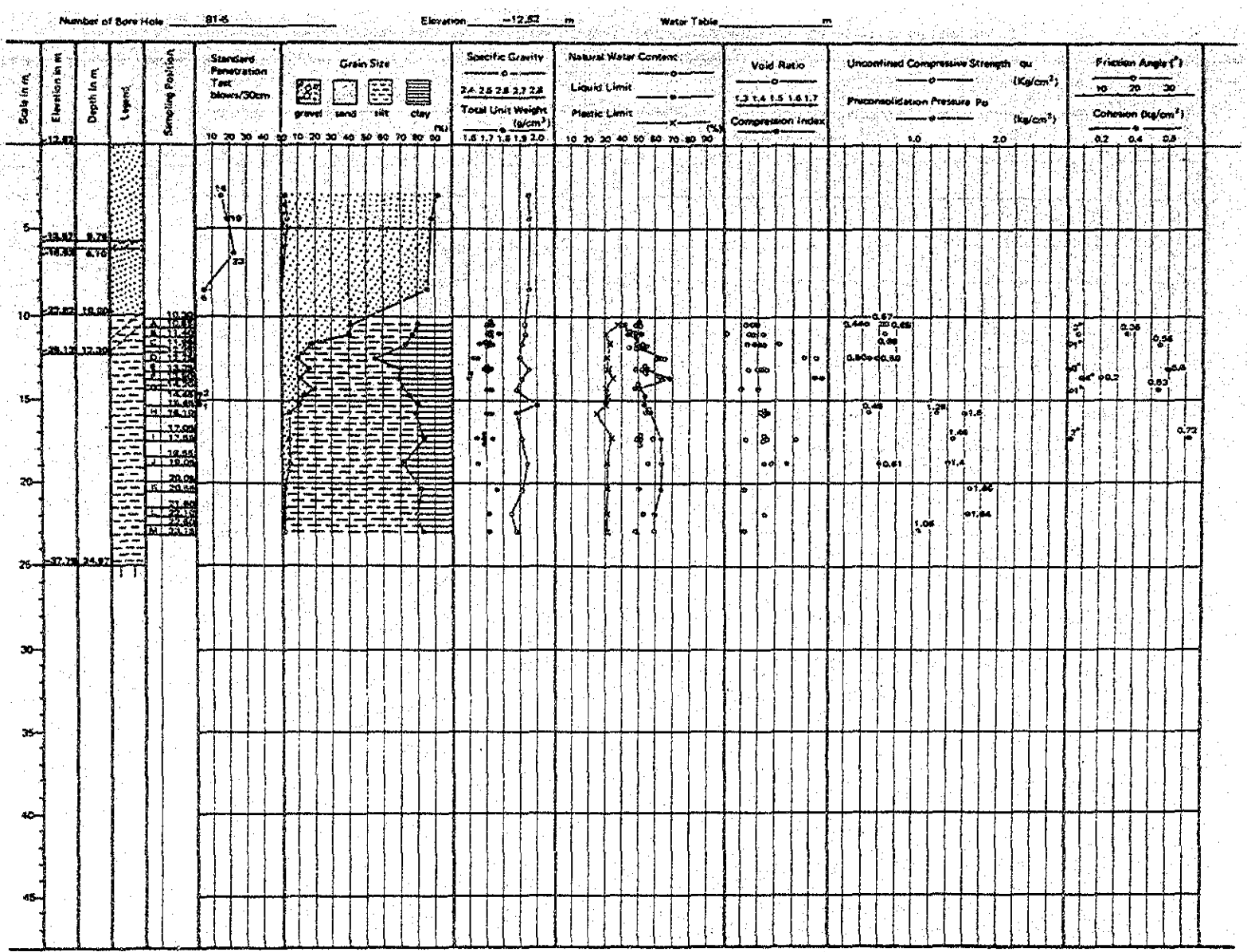

Fig. M-2 Summary of Results of Soil Tests around the Extended Breakwater (Borehole No. 81-5)

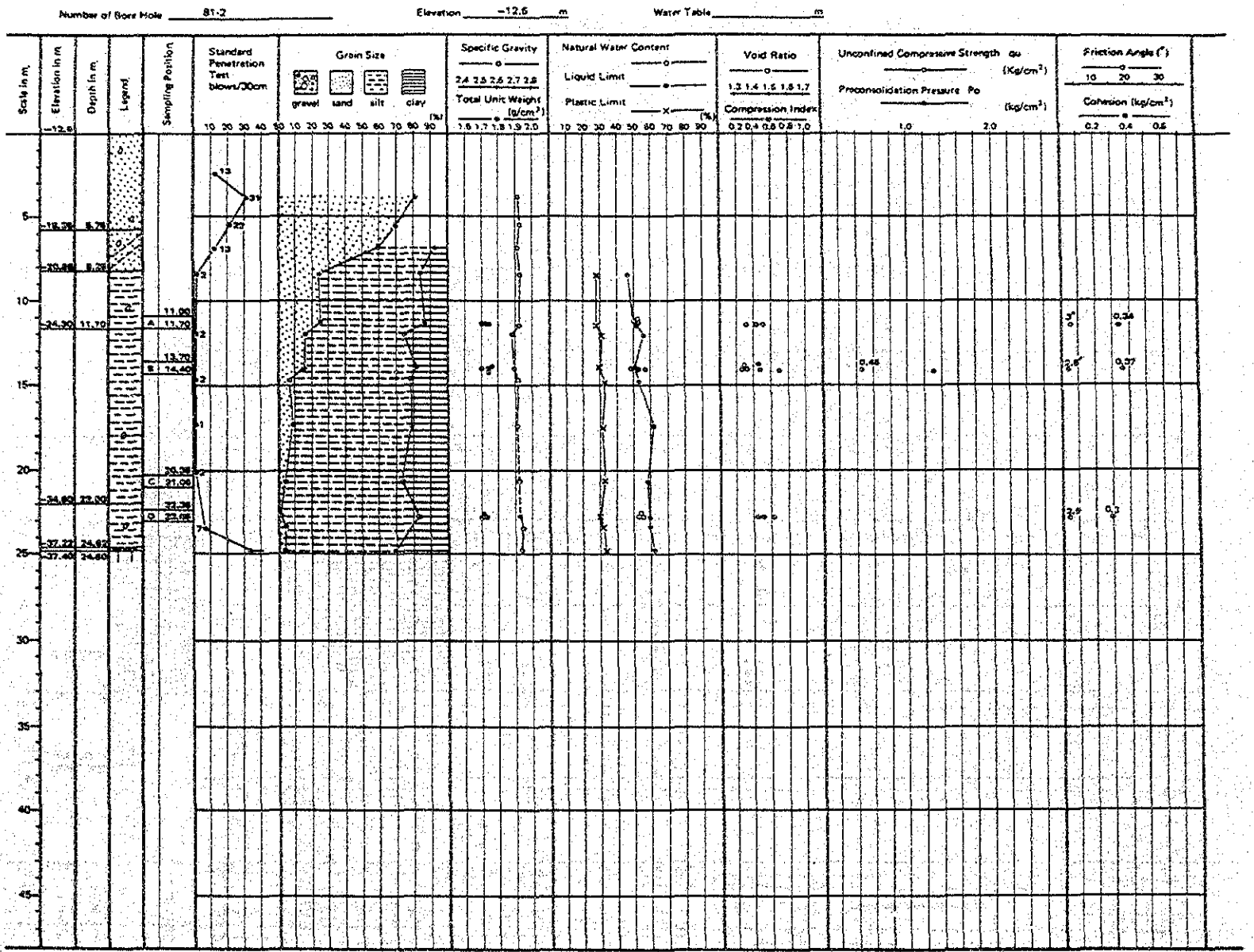

Fig. M-3 Summary of Results of Soil Tests around the Extended Breakwater
(Borehole No. 81-2)

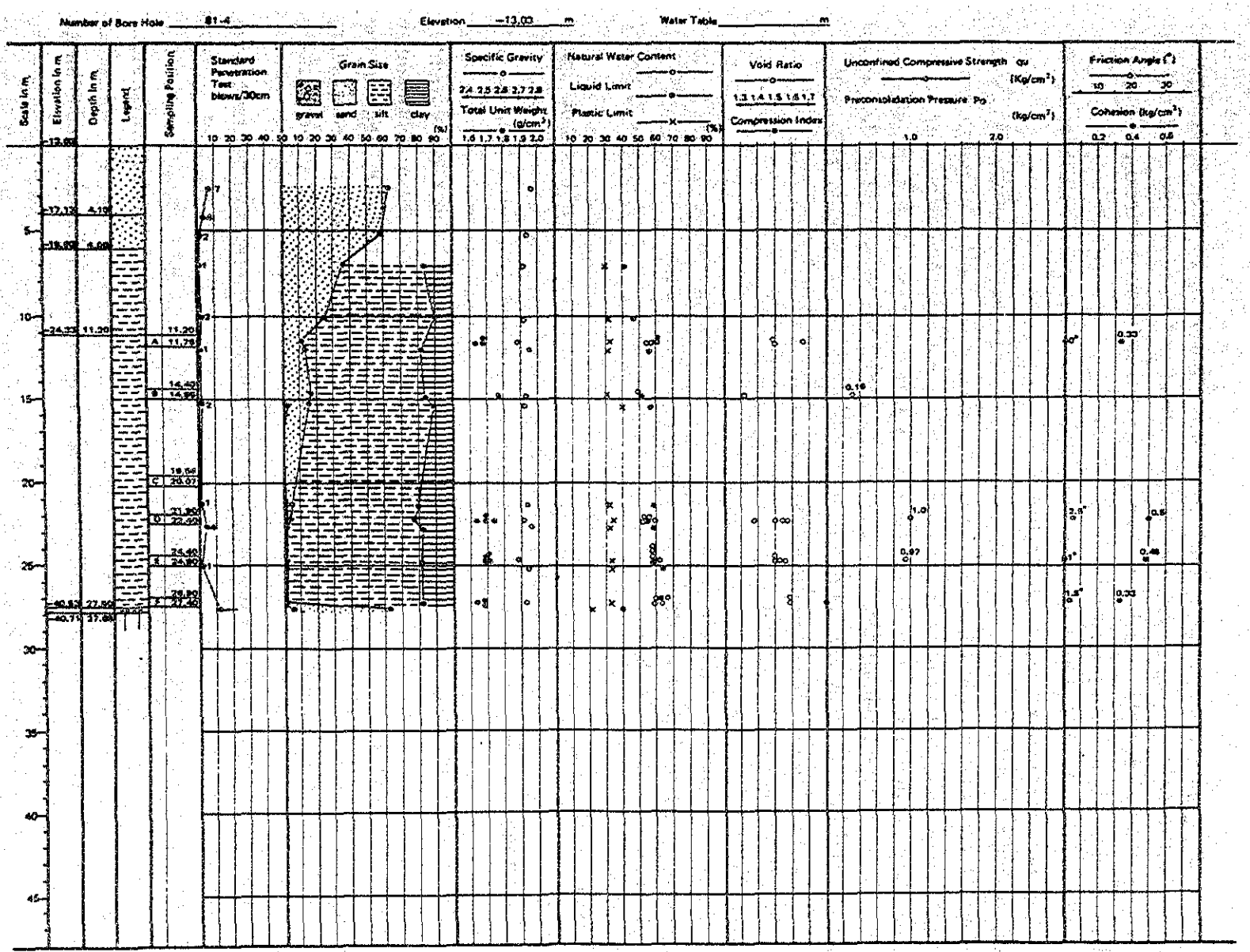

Fig. M-4 Summary of Results of Soil Tests around the Extended Breakwater
(Borehole No. 81-4)

APPENDIX 3 RESULTS OF THE NATURAL CONDITIONS STUDY

1. Results of Sounding, and Shoreline and River Surveys

In order to understand the characteristics of beach variations in the sea region surrounding the Port of Caldera, past sounding charts and lateral profiles along the seashore were collected, and hydrographic sounding and lateral surveys including a lateral survey of the Mata de Limón Inlet were performed.

Fig. M−1 shows the scope and object of each drawing.

The documents collected are listed below.

(a) Sounding Charts
  a) Overall Port of Caldera
  b) Inside the Port of Caldera
  c) Breakwater area
  d) North Caldera coastal area

(b) Lateral Profiles along the Seashore
  a) Corralillo Beach and New Beach area
  b) North Caldera coastal area
  c) Breakwater area
  d) North Caldera coastal jetty area
  e) Along Mata de Limón Bridge
  f) Inside the Port of Caldera

2. Water Current Observation

2.1 Outline

Current observation at the Port of Caldera was carried out from October 9 to November 8, 1985 at 19 locations which are shown in Fig. M−3. Of the 19 locations, 4 were continuously observed round the clock for 15 days using Ono-type current meters (OC−1) and the remaining 15 locations were continuously observed with CM−2 D type direct current reading current meters for periods ranging from 12 to 24 hours. The water depth at all observation points was 3 meters above the sea bottom.

Based on the observation data, a consolidated analysis was performed with regard to the following items.

(a) Reading of the self-registering record (OC−1 type)
(b) Flow component velocity, tidal current vector calculations and drawing execution
(c) Extraction of observed maximum values
(d) Calculation of frequency of current distribution with regard to direction and velocity of current and drawings thereof
(e) Harmonic analysis of round the clock tidal currents
(f) Preparation of tidal current ellipse current diagrams
(g) Preparation of current diagrams

a) Measured current (southward and northward currents predominating)
b) Permanent currents
c) Mean current distribution at spring tide
d) Inferred spring tide current
e) Supplement of current distribution with data obtained by CM−2 D type current meter
g) Typical curves of the four seasons

2. 2 Results of the Analysis

(1) Tidal current curves

According to a tidal current plot of the Ono-type meter data, a semidiurnal period fluctuation predominates at each of the observation points. However, at observation point O−4, the flow at the time of northward current is blocked by the Port of Caldera breakwater and the northward component becomes extremely small.

The data obtained by the CM−2 D type current meters show areas which fluctuate irregularly, but on the whole a trend similar to the data obtained by the Ono-type meter is apparent.

(2) Tidal current vectors

Tidal current vectors indicate trends similar to the conditions recorded in the tidal current curve.

(3) Observed maximum values

The observed current velocity values are subdivided by each 5° of current direction. The main direction and the anti-main direction are determined, and their respective maximum current values are noted.

As shown in Table M−1, the maximum velocity appears at point O−1 at a value of 0.5 m/s. At O−2 and O−3, the values are 0.3−0.4 m/s. At O−4, a southward current exceeding 0.4 m/s can be seen briefly at spring tide.

(4) Current frequency diagram

At the round the clock observation points, the values for the frequency of velocity distribution by tidal current direction and the mean velocity and frequency of mean distribution by direction were calculated.

According to Fig. M−3, each observation point has a predominant direction and velocity in the direction of the stream axis. At points O−1∼O−3, northward and southward velocities in a 0∼0.2 m/s range predominate, and overall current velocity is comparatively low. The velocity of the predominately southward current at point O−4 is much lower than at the other three points. A current velocity of 0∼0.1 m/s is most common.

A stream of twice the component level was observed which indicates that there is a considerably large flow in addition to the tidal current.

(5) 15 day harmonic analysis of tidal currents

A ten component harmonic analysis was performed using 15 day round the clock tidal current data. Non-harmonic constants were calculated using the harmonic constants obtained by harmonic analysis of each observation point. Table M—2 presents these non-harmonic constants.

A consideration of the correlation of maximum current velocities in light of these data indicates that a stream of about twice the level of the tidal current component is observable, and that the non-tidal current stream is large.

(6) Tidal current ellipse

As stated in (5) above, the semidiurnal components at each point are large. Hence the Spring Tropic tidal current hodograph varies in roughly the same manner as the ellipse of the M_2 tidal current.

A principal 4 component diagram (M_2, S_2, K_1, D_1) and a Spring Tropic tidal current ellipse diagram are shown in Fig. M−4(1)~M−4(4)

(7) Current diagrams

A study of current diagrams in which the high water time at the Port of Caldera is used as a standard reveals a southward current at the time of high water which becomes a northward current 1 hour before low water.

The southward current reaches maximum velocity about 1 hour after high water, with a velocity at points O—1 ～ O−3 of 0.13 ～ 0.22 m/s. The northward current begins to turn about 2 hours before high water, and subsequently shifts to a southward current.

The northward current reaches a maximum velocity of 0.13 ～ 0.20 m/s. about 1 hour after low water. At this time, a reversing backflow is created immediately behind the backwater near O−4 ; however, its velocity is minimal in comparision to that at points O−1 ～ O−3. In preparing the current charts, the observation values obtained with the CM−2 D type current meters are used to supplement the current distribution diagrams.

The typical current distributions at the time of northward current and southward current at the Port of Caldera are shown in Fig. M−5, and Fig. M−6 shows the current distribution during maximum northward and southward currents.

(8) Permanent current

According to Fig. M−6(1) and Fig. M−7, the permanent currents at points O−1 ～ O−3 are minimal and the current directions of the observation points are not uniform. As indicated by the vector diagrams, at O−4 there is a southward current of 0.04 m/s. due to a one-sided tide phenomenon, and the current velocity value at this point is roughly equivalent to the tidal current component.

(9) Typical curves of the four seasons

A study of the typical curves of the four seasons shows that the main directions of the tidal currents at the observation points are roughly northward. It is clear that the southward current reaches maximum velocity 1 hour after high water at the Port of Caldera, and the

northward current reaches maximum velocity 1 hour after low water. The aberration in tide time between the observation points is extremely low, and the current becomes strong and weak in concert over the entire region.

The diurnal component is small in comparison with the semidiurnal component, hence even in summer and winter diurnal inequality is small and the fluctuation of the semidiurnal period is significant.

3. Tide Observation Results

An examination of the harmonic analysis using the observation records of the Port of Caldera is given in CHAPTER IV, 3.3.

4. Wave Observations Results

Significant wave frequency distribution and cumulative probability distribution using wave records of the Port of Caldera are given in CHAPTER IV, 3.1.

5. Results of Sediment Sampling and Analysis

The documents collected in Caldera were used to perform a grading analysis and to prepare a grain size accumulation curve at MOPT's soil test laboratory.

Table M−2 displays values found according to the grain size accumulation curve for sorting coefficient and the polarized distortion degree which become an index of the bottom materials grading characteristics.

Sorting coefficient $S_0 = d_{75}/d_{25}$

Polarized distortion degree $S_k = d_{75} \times d_{25}/(d_{50})^2$

Where, d_{50} : cumulative 50% corresponding grain size (median diameter)
d_{75} : cumulative 75% corresponding grain size
d_{25} : cumulative 25% corresponding grain size

According to the index of the bottom materials grading characteristics, the median grain diameter at the point S−4 in front of the quaywall is 0.14 mm, indicating a smaller value than at other locations. The sorting coefficient is 2.40 which means that the slope sorting of the bottom materials is poor.

At locations other than S−4, a distribution of median diameter between 0.24 mm ~ 0.34 mm is found, the mean of which is about 0.3 mm. The sorting coefficient is between 1.4 and 1.7, which indicates a normal slope sorting of bottom materials. Near the tip of the breakwater, grain size is slightly larger, and a trend towards favorable slope sorting of bottom materials may be observed. However, considering these bottom materials to be similar to those found at locations other than S−4 will not pose any problems.

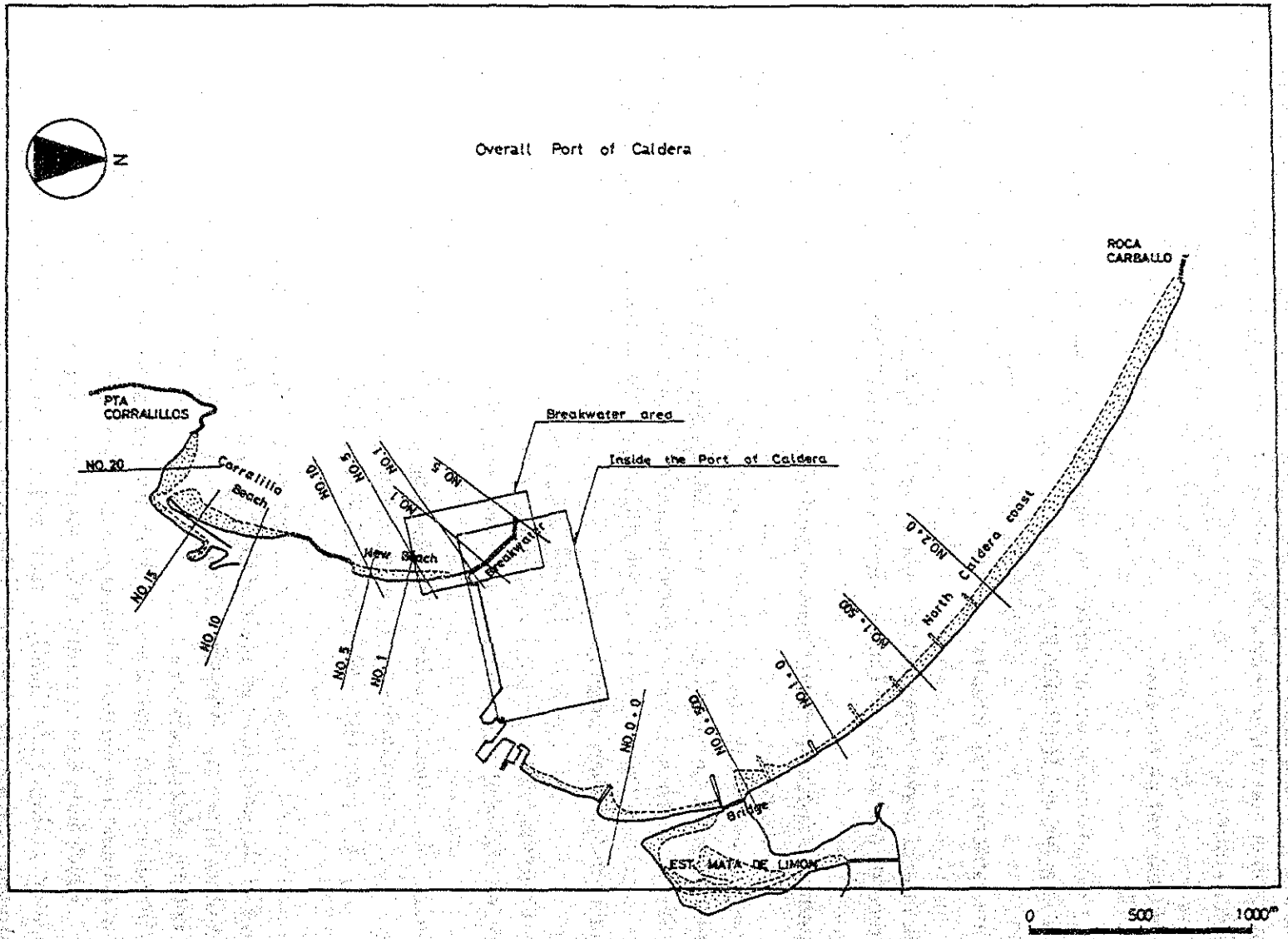

Fig. M-1 Location Map of Sounding and Topography Survey along the Shoreline

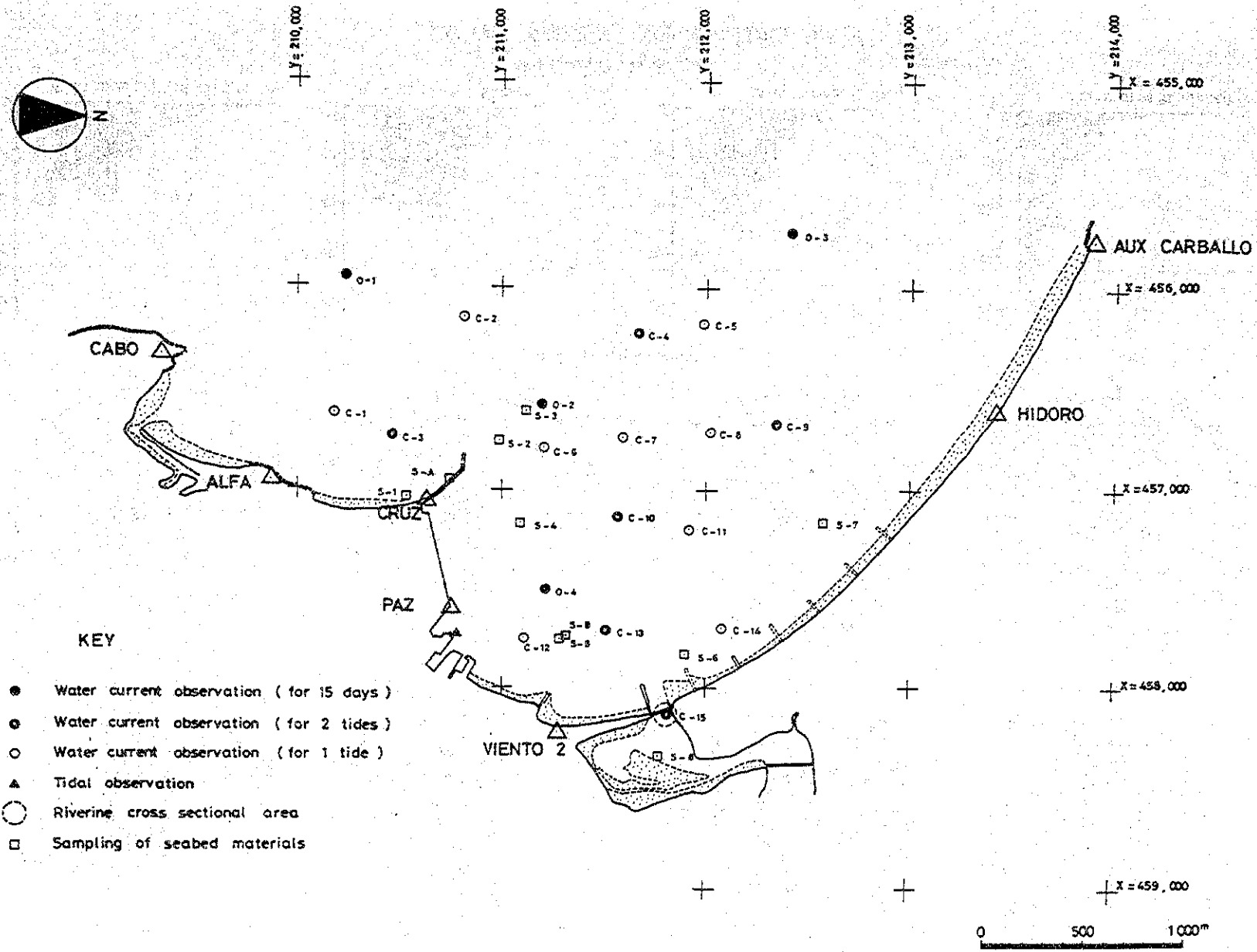

Fig. M-2 Location Map of Field Surveys

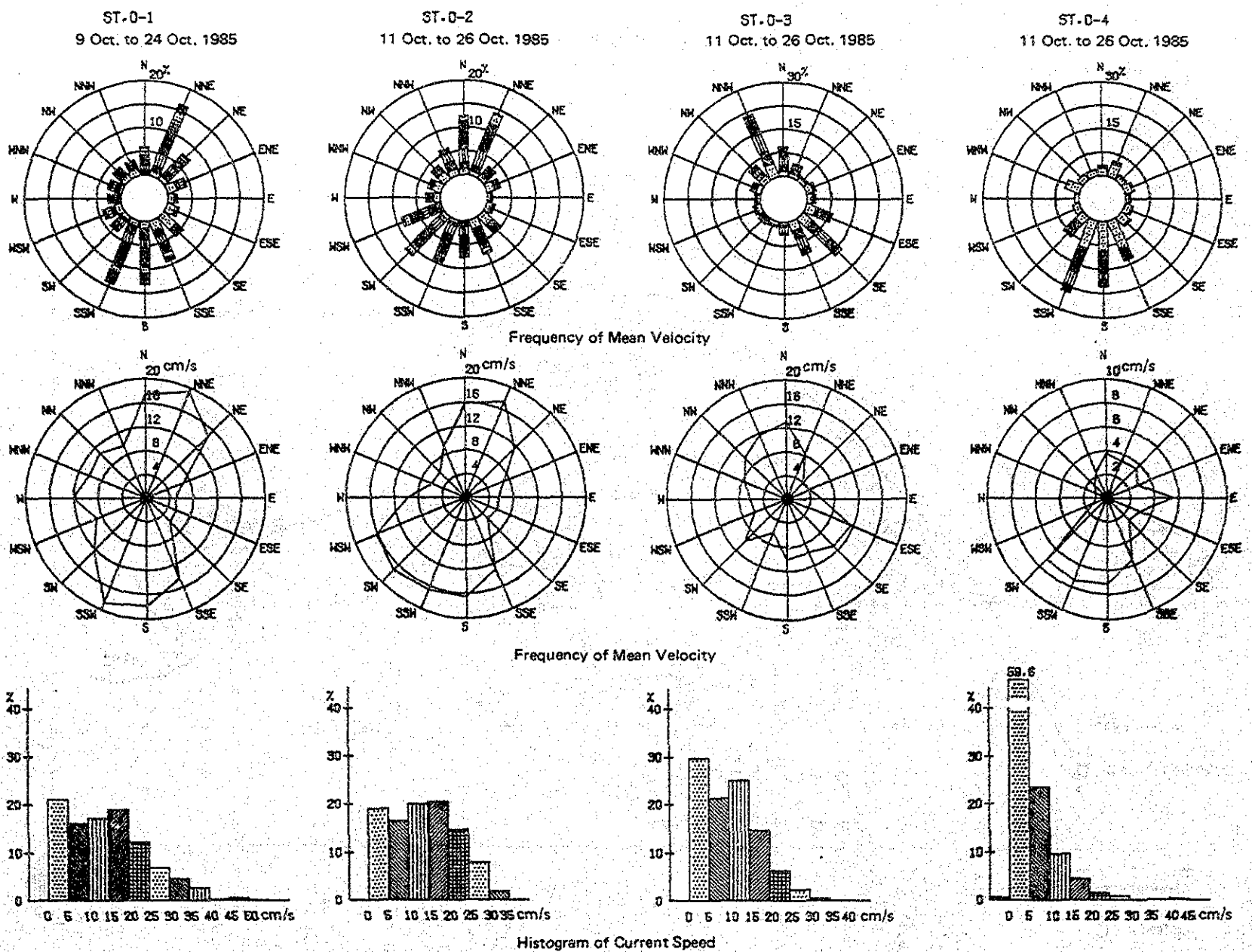

Fig. M-3 Frequency of Current Distribution

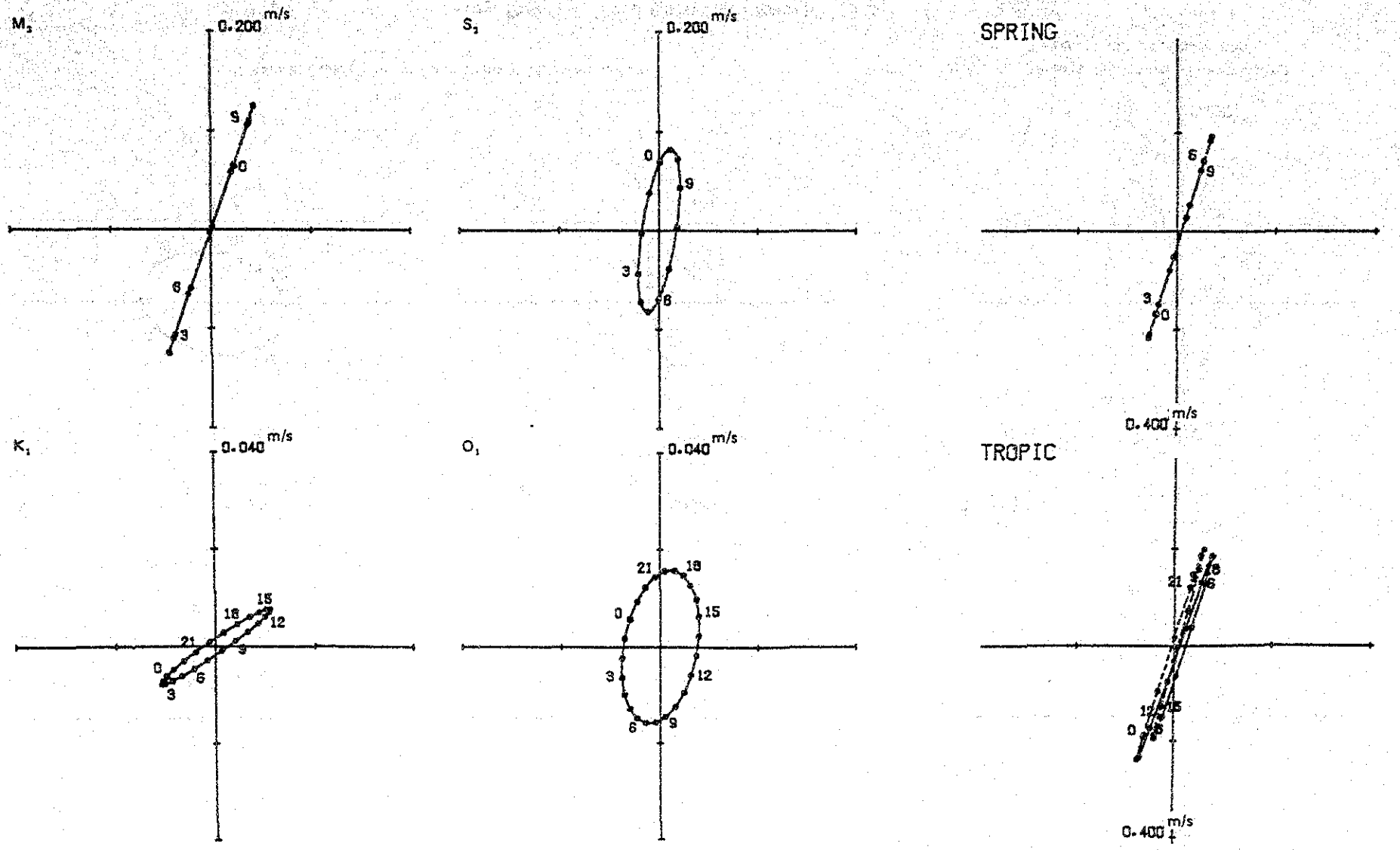

0 Hour is Transit Time of Component at Observation Point

0 Hour is High Water Time at Caldera
Period: 9 OCT. to 24 OCT. 1985

Fig. M-4 (1) Tidal Current Ellipse ST. O-1

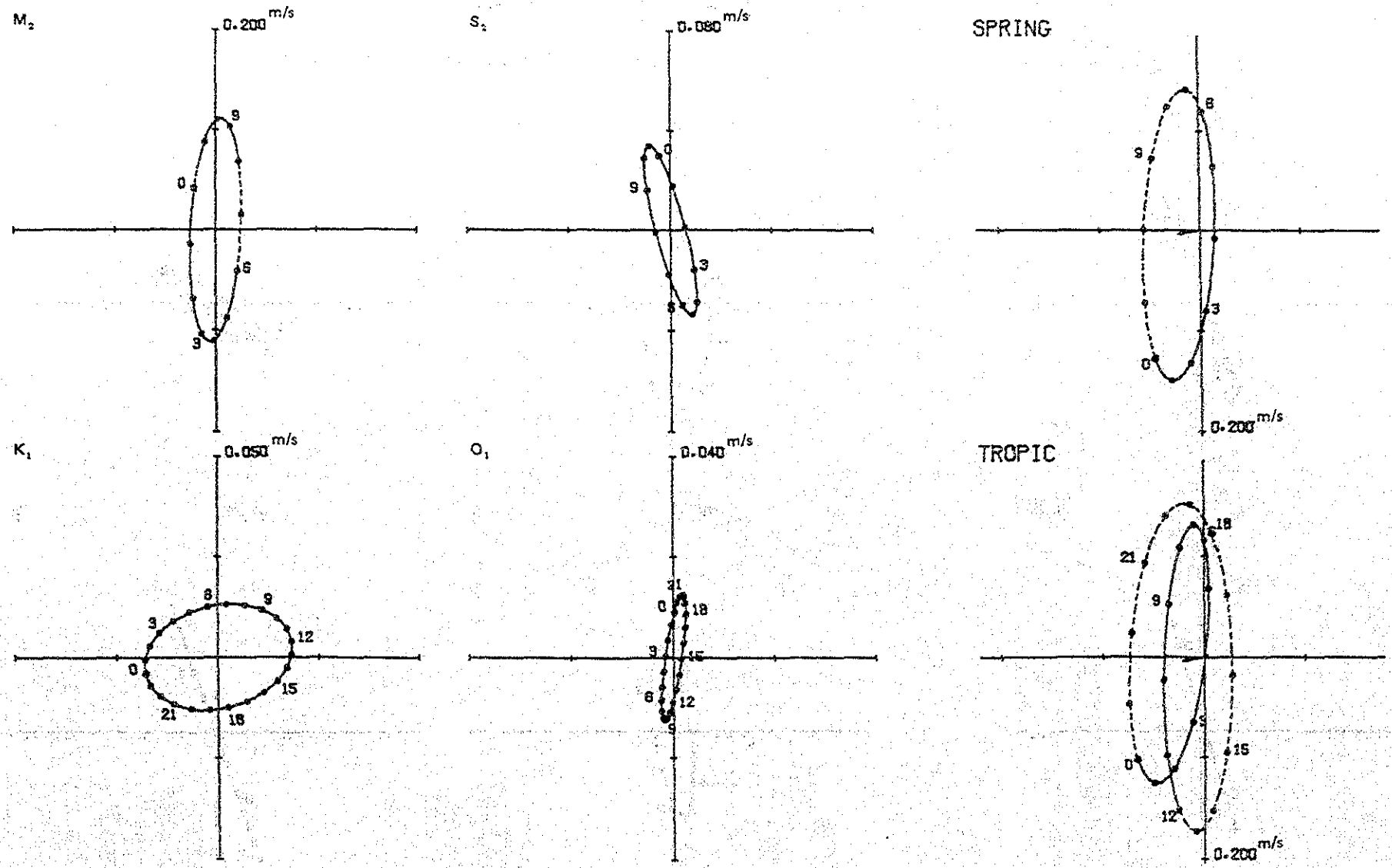

Fig. M-4 (2) Tidal Current Ellipse ST. O-2

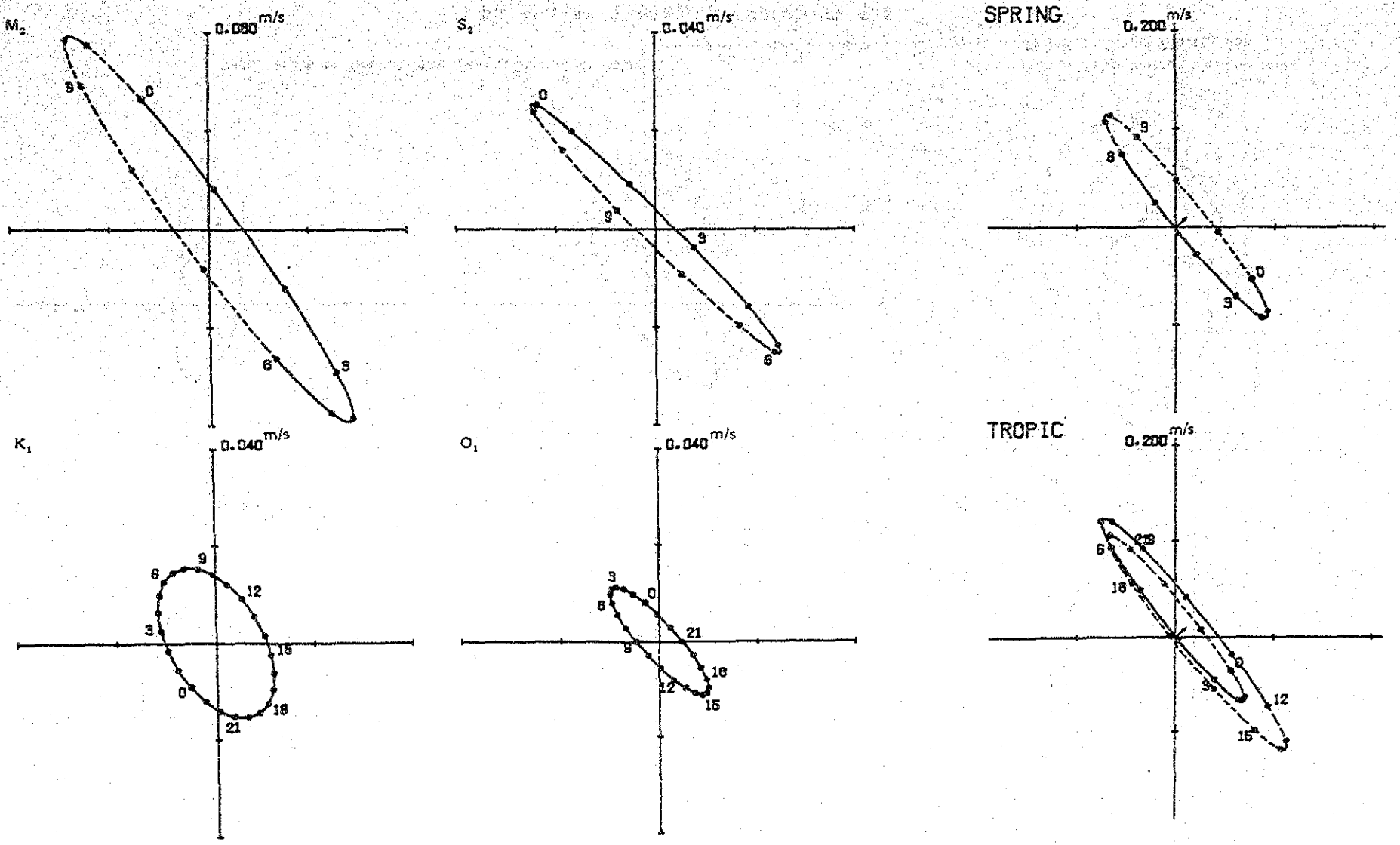

0 Hour is Transit Time of Component at Observation Point

0 Hour is High Water Time at Caldera
Period: 11 Oct. to 26 Oct. 1985

Fig. M-4 (3) Tidal Current Ellipse ST. O-3

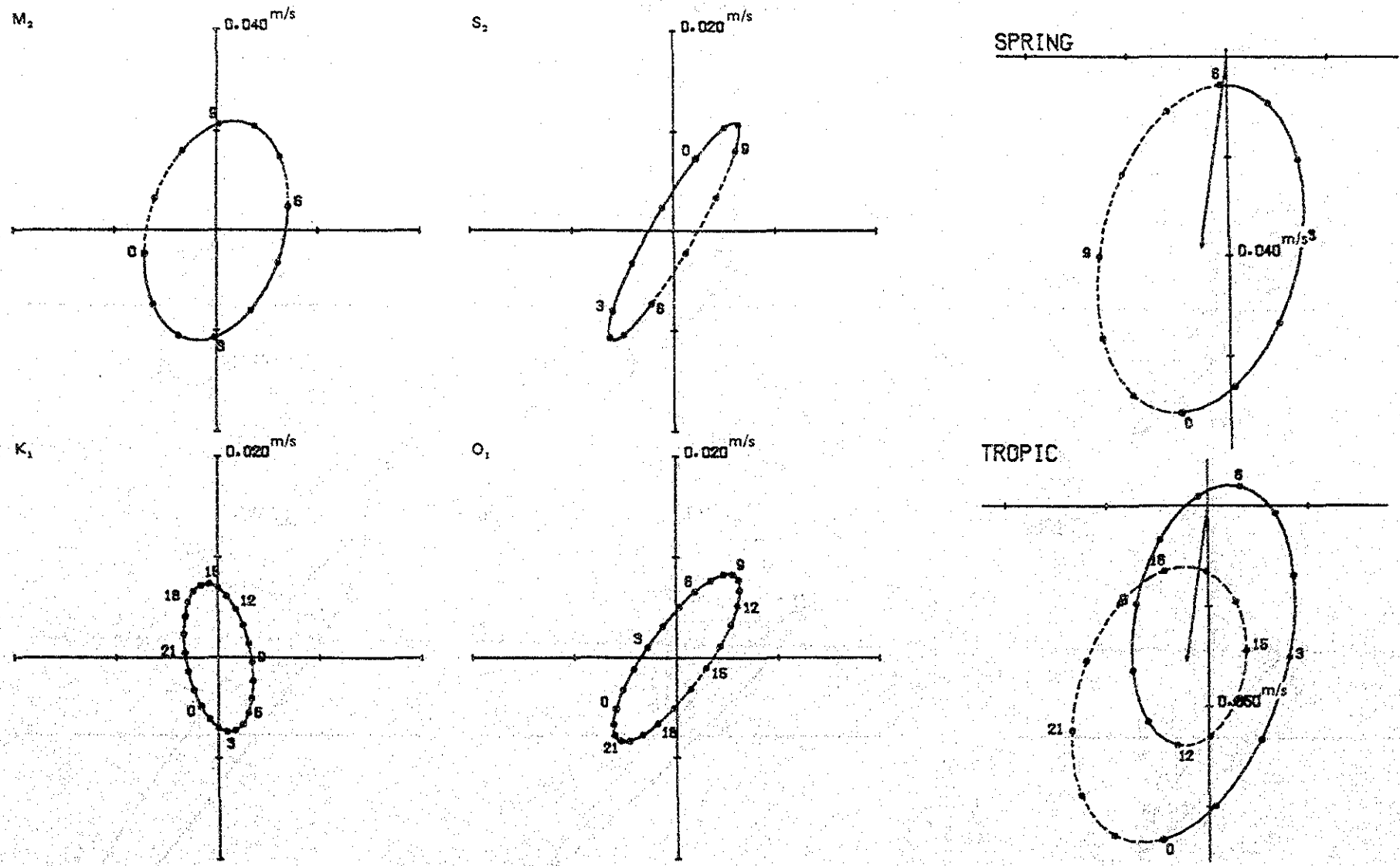

0 Hour is Transit Time of Component at Observation Point

0 Hour is High Water Time at Caldera
Period: 11 Oct. to 26 Oct. 1985

Fig. M-4 (4) Tidal Current Ellipse ST. O-4

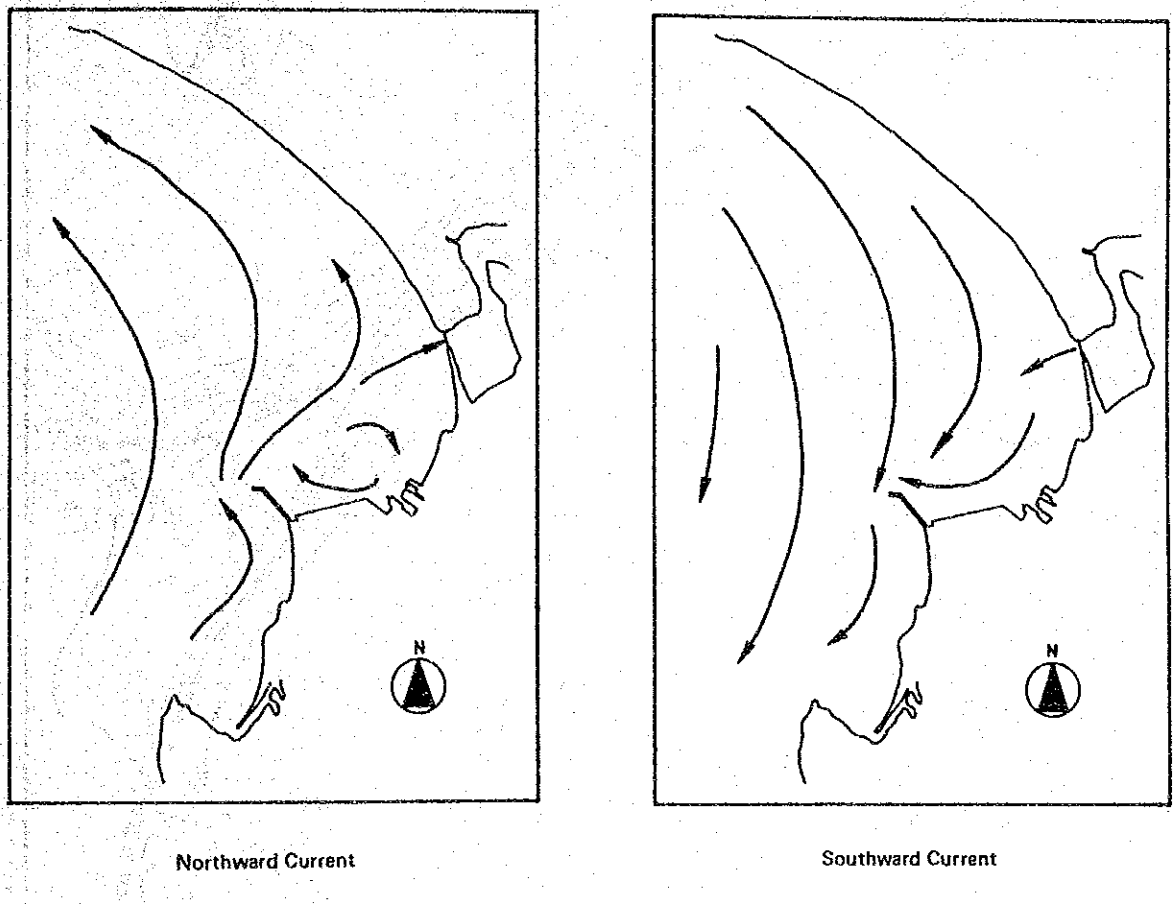

Fig. M-5 Typical Tidal Current

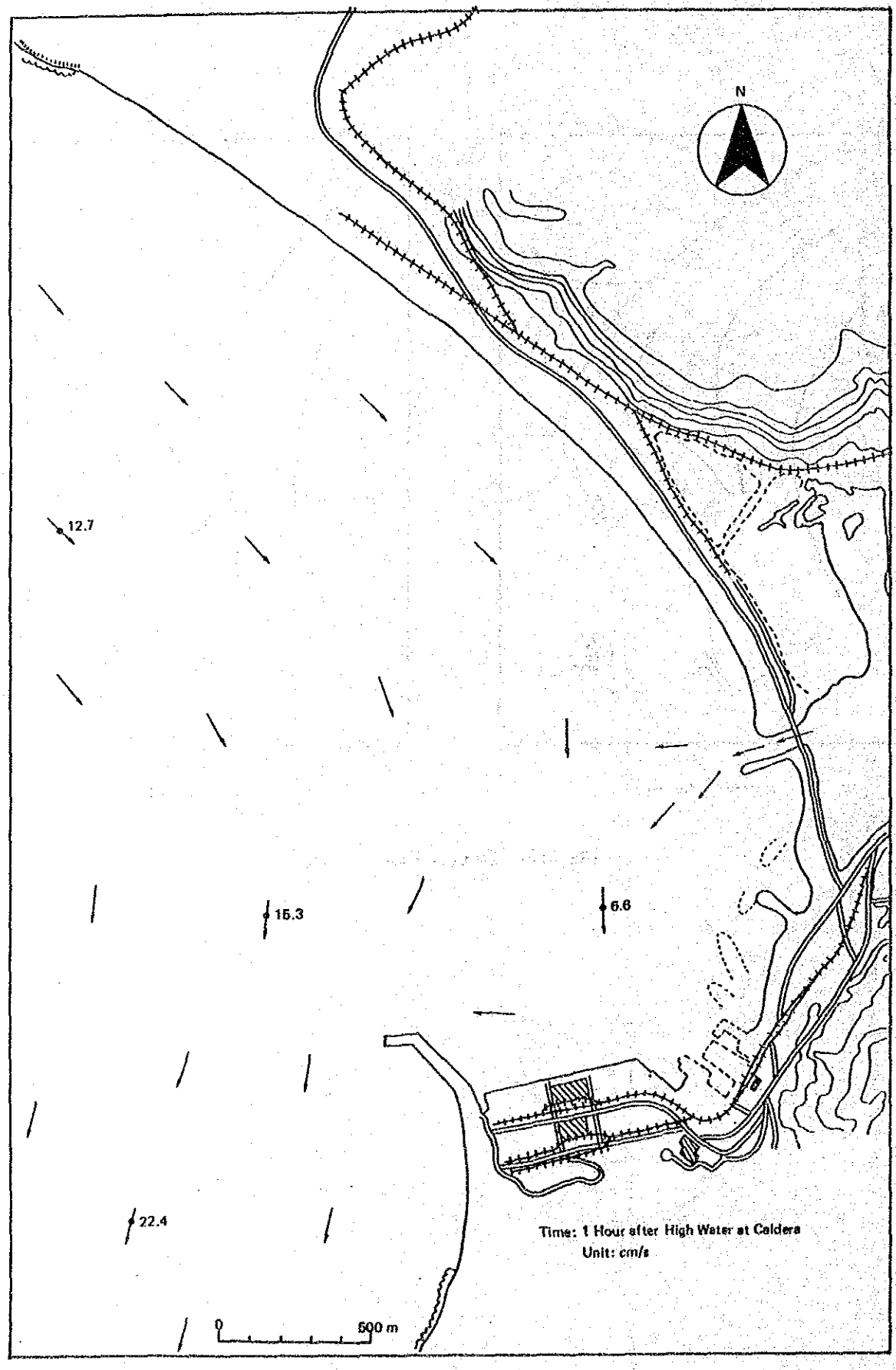

Fig. M-6 (1) Main Current Distribution at Spring Tide

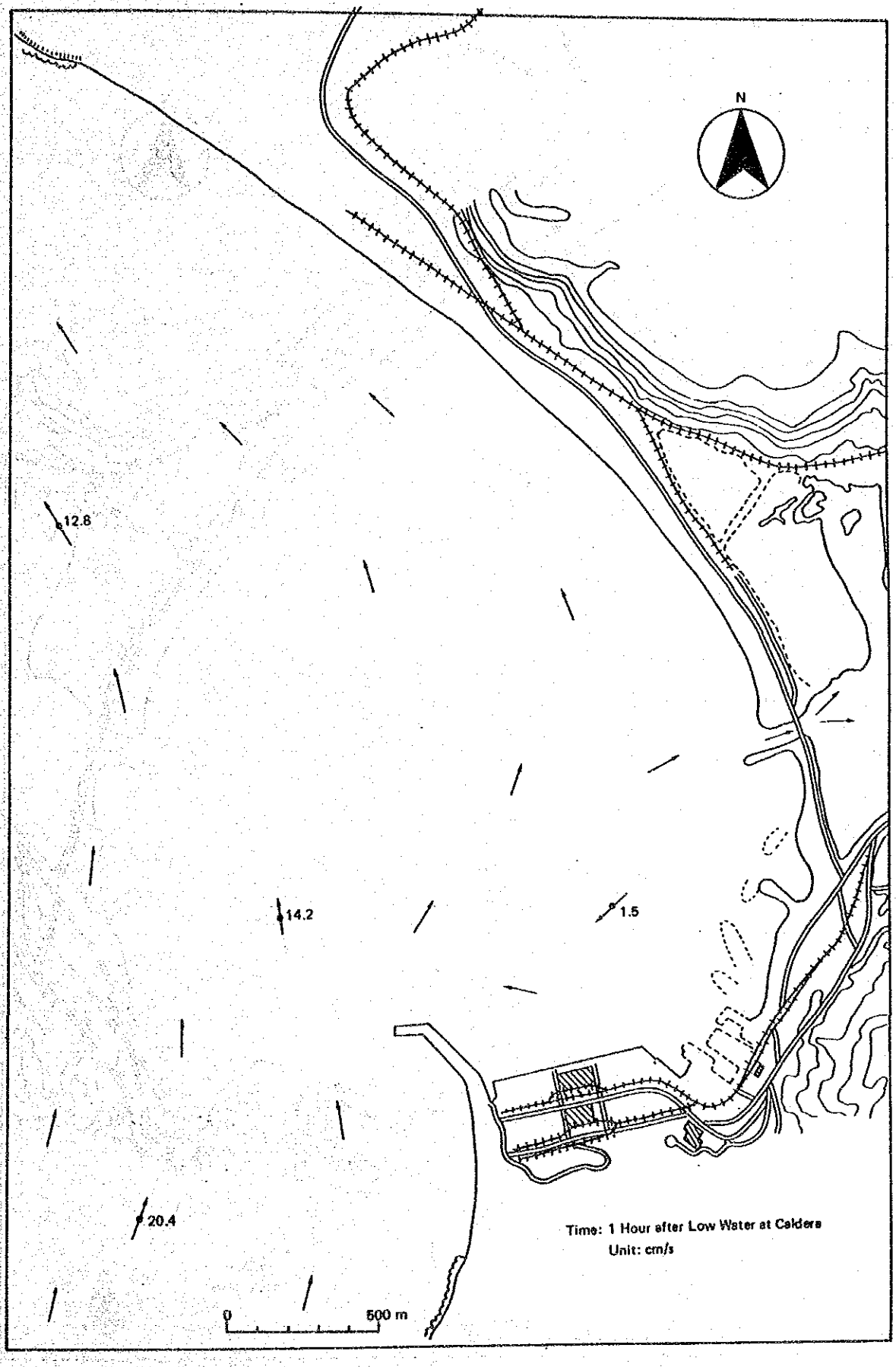

Fig. M-6 (2) Main Current Distribution at Spring Tide

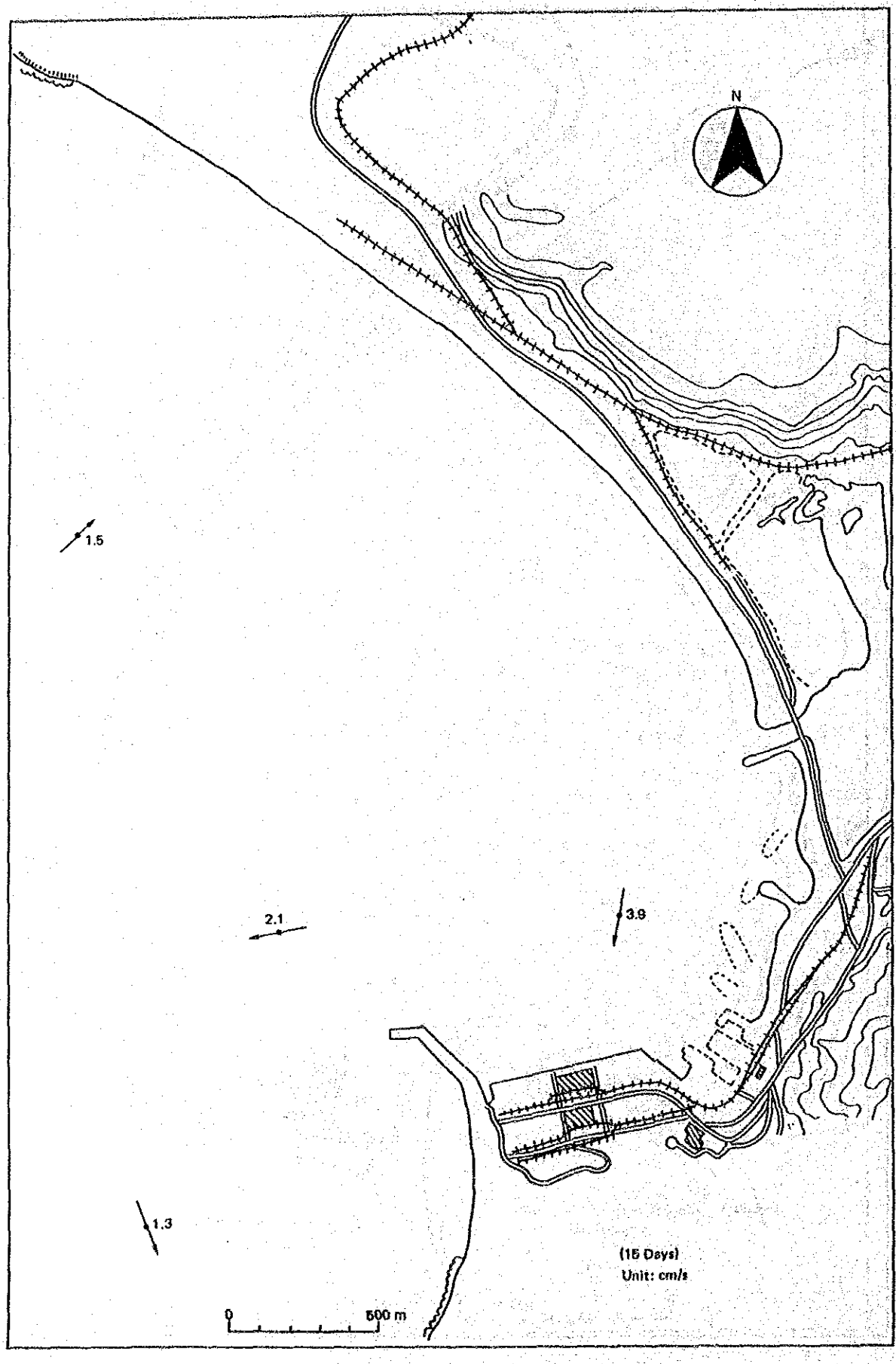

Fig. M-7 Permanent Current

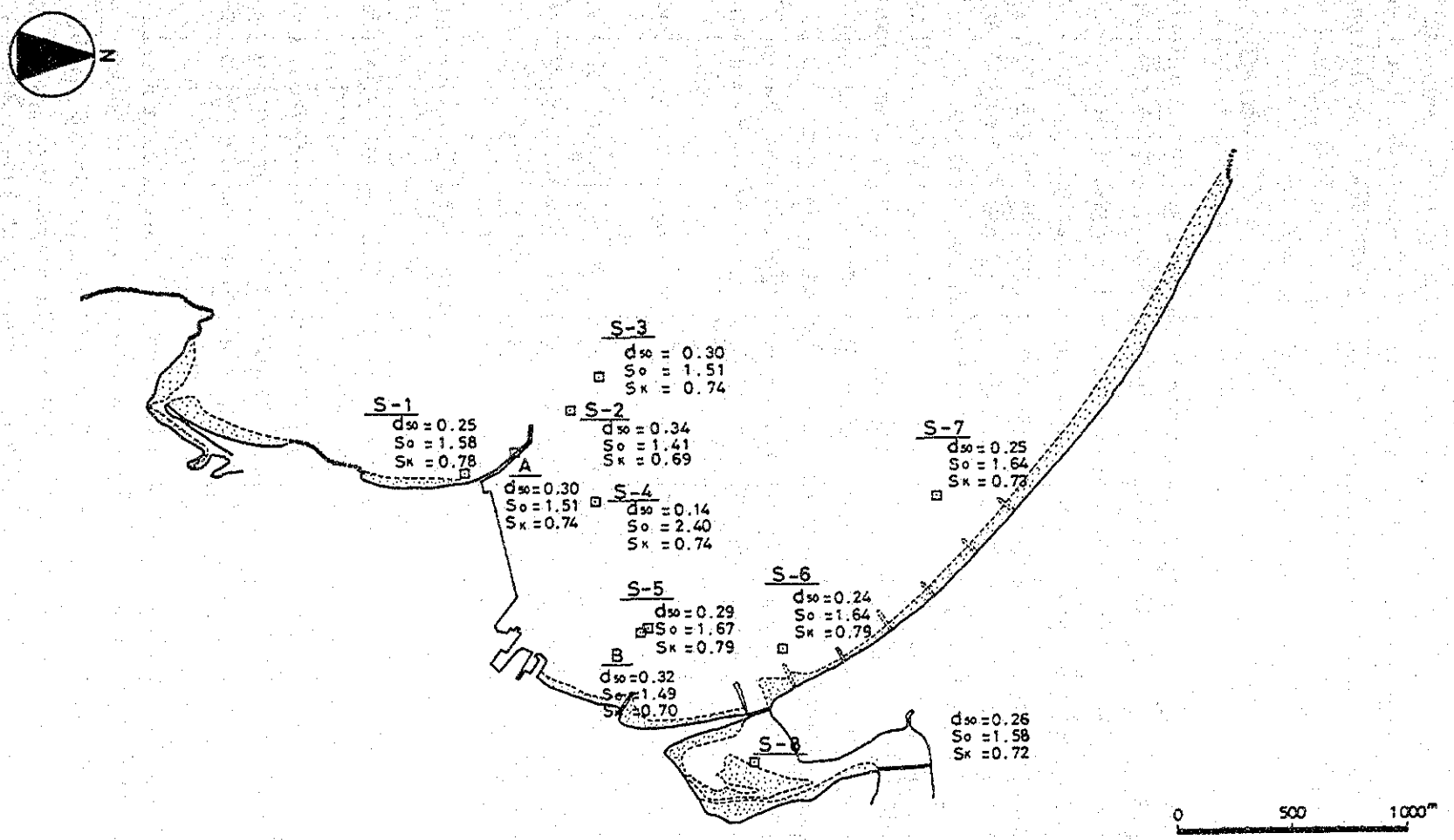

Fig. M-8 Bottom Materials Grading Characteristics

Table M-1 Maximum Current Velocity Values

Observation point	Main direction	Maximum observed velocity in main direction			Maximum observed velocity in anti-main direction		
		Time of appearance	Velocity	Direction	Time of appearance	Velocity	Direction
O—1	20°	16 Oct.22:20	0.56m/s	12°	14 Oct.5:20	0.45m/s	178°
O—2	15°	20 Oct. 2:20	0.33	22°	19 Oct. 8:20	0.34	221°
O—3	340°	26 Oct. 9:00	0.38	350°	13 Oct. 4:00	0.34	114°
O—4	20°	16 Oct. 6:20	0.17	85°	15 Oct. 5:00	0.45	181°

Table M-2 Non-harmonic Constants

Observation point	M_2+S_2	K_1+O_1	$M_2+S_2+K_1+O_1$	$\frac{K_1+O_1}{M_2+S_2}$	$\frac{K_m}{29}$
Tide	1.295m	0.135 m	1.427m	0.10	2.8h
O—1	21.5m/s	12.6m/s	24.1m/s	0.12	10.4
O—2	14.3	17.0	17.0	0.19	10.0
O—3	13.2	16.4	16.4	0.24	10.6
O—4	3.4	5.1	5.1	0.50	8.5

APPENDIX 4. IMMEDIATE BREAKWATER EXTENSION WORKS

This information concerning the immediate extension works of the breakwater is prepared by the Japanese Study Team (JST) of JICA in compliance with the Minutes of Meeting between DGOPF/MOPT and JST dated November 18, 1985. The meeting was held in San José, Costa Rica.

1. Introduction

The littoral drift at the Port of Caldera which causes the forward movement of the shoreline of New Beach due to drift sand coming from the south is quite rapid. The depth at the head of the breakwater has become very shallow, about 3 m to 5 m ; consequently, the volume of drift sand going round the head of the breakwater is considerable.

Furthermore, the annual rate of littoral drift has been increasing. It is estimated that between August 1982 and August 1984 64,000 m^3 of sand entered the harbour from the south. However, from August 1984 to August 1985 an estimated 95,000 m^3 of sediment entered the harbour. Thus, the annual rate of littoral drift in 1984/85 was roughly 3 times the average annual rate over the preceeding two years.

Among the various countermeasures to prevent sedimentation in the harbour, extension of the breakwater is clearly the most important and should be completed as soon as possible. MOPT has been working at extending the breakwater for some time, but it is necessary to expedite the construction works to prevent further sedimentation of the harbour.

2. Center Line and Extension Length of the Breakwater

As of November 1985, the length of the wing jetty was 115 m. The wing jetty should be extended to 150 m, and the center line of the extension works should be in accordance with the center line of the existing wing jetty.

3. Improvenment of the Construction Procedure

(1) Improvenment of the structural sections

When constructing a rubble mound breakwater on a sandy base, it is necessary to take sufficient countermeasures to prevent scours and sinkages at the base of the breakwater , particularly at the toe. The main countermeasures for the construction at Caldera are :

(a) Rubble stones shall be thrown in advance, and these rubble stones which will sink due to wave action will stabilize the base of the breakwater. The sinkage of the rubble stones shall be estimated as about 2 m. Furthhermore, the total volume of rubble stones necessary shall be calculated with an allowance of 20%.

(b) As armour stones rapidly sink if they are placed directly on the sand, the armour stones shall be carefully placed on the rubble foundation.

(c) The toe of the rubble shall be sufficiently long to prevent sinkage of armour stones which would otherwise be caused by scours of the toe of the rubble founda-

tion. Accordingly, we propose that the extension be constructed as shown in Figure 1.

(2) Improvenment of construction schedule and construction management

In order to build the extension successfully, it is crucial to prepare a detailed construction schedule and to execute the construction works on schedule. Although the machinery at the site is limited, any delay in the placement of the stoned would cause a serious disruption of the project. The proposed construction schedule is presented as Table 1. The construction shall proceed as follows :

(a) First of all, the rubble mound shall be constructed in advance. This mound will soon be deformed by wave action.

(b) In accordance with the construction schedule, additional rubble stones shall then be placed, and the final rubble mound shall be formed (see Fig. 2).

(c) Thereafter, at intervals of about 5 m, the armour stones shall be set without delay (see Fig. 3).

(d) Construction steps 8 and 9 (in Fig. 3) shall be executed from the head of the breakwater as the final part of the 150 m wing jetty.

(e) Armour stones of 6~8 tons unit weight shall be temporarily placed at the head of the breakwater. A slope of one to one shall be used for the placement. The armour stones shall be directly placed on the rubble foundation.

(f) The construction volume at the breakwater head is also shown in Figs. 2 and 3.

(g) The production volume of the 6~8 ton armour stones is estimated as 50 m^3/day based upon the field survey.

(h) The two items noted below are the most important items in the construction schedule :

1) The 120 ton lifting capacity truck crane shall be operated on the breakwater for the placement of stones.

2) The 6~8 ton unit weigth armour stones shall be produced by Komatsu wheel loaders at an average volume of 50 m^3/day.

The production and construction works shall take place simultaneously. The production period is estimated as 105 days.

(i) Any reduction in the operation rates of the truck crane (P & H) or the wheel loader (Komatsu) would create a bottleneck in the construction. As construction delays must be avoided at all costs, it is essential to create a regular maintenance system for these machines and to ensure that sufficient spare parts are available on site.

(3) Improvement of the armour stone placement procedure

The stability of breakwater against wave action primarily depends on the accuracy of the armour stone placement.

Generally, the requisite weight of an armour stone is calculated using Hudson's formula.

$$W=\frac{r_r H^3}{K_D(S_r-1)^3\ \cot\alpha}$$

Where, W : Requisite weight of an armour stone
γ_r : Unit weigth of the armour stone in air
S_r : Specific gravity of the armour stone in sea water
α : Angle of the slope to the horizontal plane
H : Design wave height ($H_{1/3}$)
K_D : Constant determined by the armouring material and damage rate

The K_D value in Hudson's formula indicates the stability of each individual armour unit. This value changes greatly depending on the accuracy of the armour stone placement. When the accuracy is better, the K_D value is higher. The present procedure of the armour stone placement seems to have some problems.

The method described below should be followed.

(a) A placement table for the operator of the truck crane should be prepared for the accurate placement of the armour stone. This can be made as follows.
  a) All locations of the armour stone to be placed will be decided by the planned breakwater plane and sectional figures.
  b) These locations can be represented by the boom length and the lifting angle of the boom.

(b) The operator will place each armour stone setting the boom length and lifting angle at the same values indicated on the table in Fig. 4.

The accuracy of the armour stone placement will increase using this method.

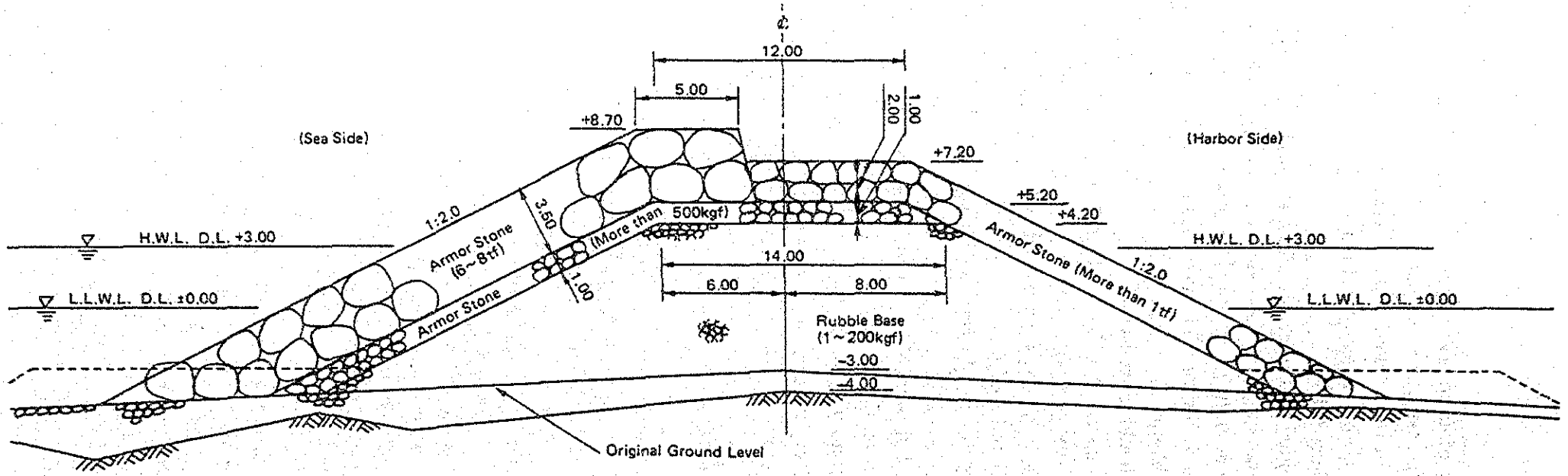

Fig. 1 Standard Cross Section of the Breakwater

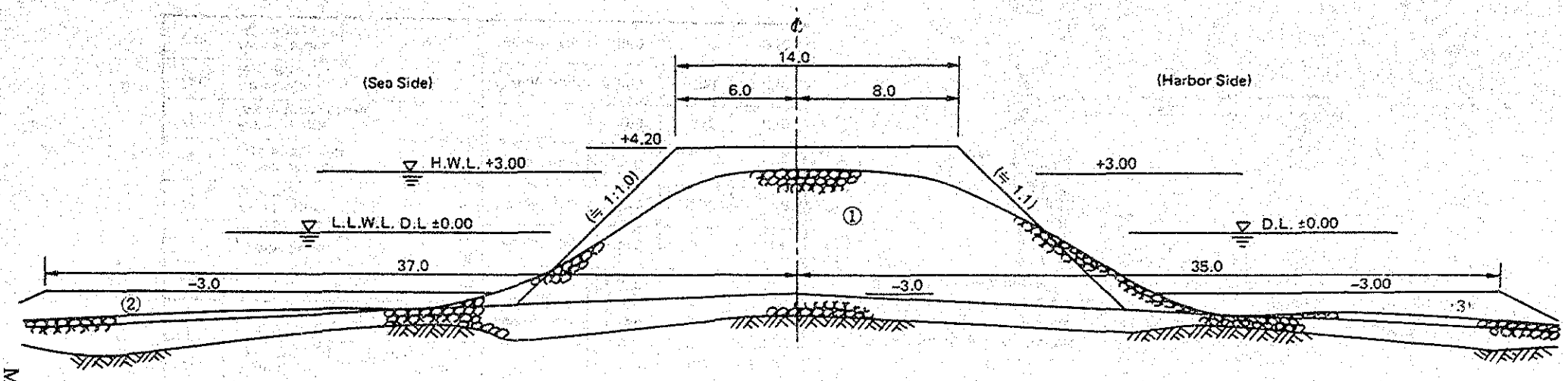

Construction Volume

Order	Material	Construction Machine	Capability	Construction Volume (m³)		
				Trunk	Head	Total
(1)	Rubble Stone (1 ~ 200 kgf)	Bulldozer (Komatsu)	500 m³/day	7,280	0	7,280
(2)	"	Truck Crane (120tf, P/H)	250 m³/day	840	4,520	6,445
(3)	"	"	"	1,085		

Note: (1) ~ (3) show the order of construction

Fig. 2 Preceding Rubble Foundation Subjected to Wave Erosion (Including the Estimated Deformation)

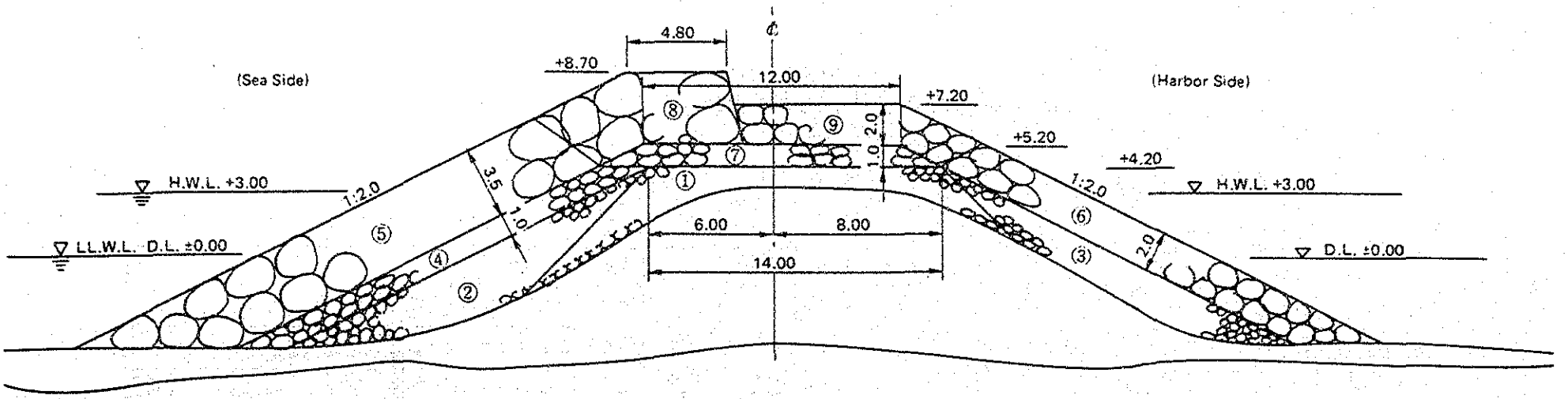

Construction Volume

Order	Material	Construction Machine	Capability	Construction Volume (m^3)		
				Trunk	Head	Total
(1)	Rubble Stone (1 ~ 200 kgf)	Bulldozer (Komatsu)	400 m^3/day	1,400	800	2,200
(2)	〃	Trunk Crane (120tf, P/H)	250 m^3/day	1,190	600	2,840
(3)	〃	〃	〃	1,050		
(4)	Armor Stone (More than 500kgf)	〃	160 m^3/day	770	530	1,300
(5)	Armor Stone (6 ~ 8tf)	〃	140 m^3/day	2,240	1,200	3,440
(6)	Armor Stone (More than 1tf)	〃	160 m^3/day	1,540	0	1,540
(7)	Armor Stone (More than 500kgf)	〃	〃	490	340	830
(8)	Armor Stone (6 ~ 8tf)	〃	140 m^3/day	1,050	600	1,650
(9)	Armor Stone (More than 1tf)	〃	160 m^3/day	840	0	840

Notes:
Notes:
1) ① ~ ⑨ shows the order of construction
2) Items ⑧ and ⑨ are constructed from the top of the breakwater
3) Armor stones (6 ~ 8T) are temporarily installed at the head of the breakwater

Fig. 3 Construction Procedure of the Breakwater

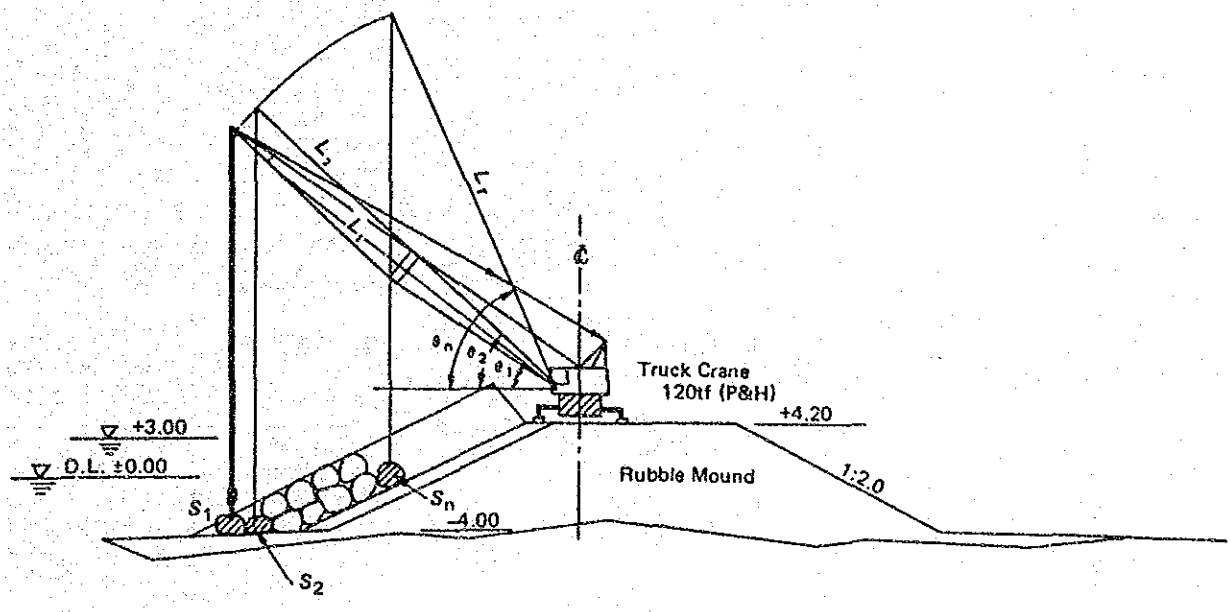

Table for Armor Stone Placement

Line	θ, L	S_1	S_2		S_n
1	θ	$\theta_{1.1}$	$\theta_{1.2}$		$\theta_{1.n}$
	L	$L_{1.1}$	$L_{1.2}$		$L_{2.2}$
2	θ	$\theta_{2.1}$	$\theta_{2.2}$		$\theta_{2.n}$
	L	$L_{2.1}$	$L_{2.2}$		$L_{2.n}$
⋮					
m	θ	$\theta_{m.1}$	$\theta_{m.2}$		$\theta_{m.n}$
	L	$L_{m.1}$	$L_{m.2}$		$L_{m.n}$

Fig. 4 Method of Armour Stone Placement

Table 1 Construction Schedule of the Extended Breakwater (L = 35 m)

Construction Step / Date	The Order of the Construction	Material	Construction Machine	Construction Volume (m^3)	Capability (m^3/day)
Preceding Rubble Foundation (Fig. 2)	①	Rubble Stone (1~200 kgf)	Bulldozer	7,280	500
	②, ③	〃	Truck Crane	6,445	250
Completed Cross Section of the Breakwater (Fig. 3)	①	〃	Bulldozer	2,200	400
	②, ③	〃	Truck Crane	2,840	250
	④	Armor Stone (More than 500kgf)	〃	1,300	160
	⑤	Armor Stone (6 ~ 8tf)	〃	3,440	140
	⑥	Armor Stone (More than 1tf)	〃	1,540	160
	⑦	Armor Stone (More than500kgf)	〃	830	160
	⑧	Armor Stone (6 ~ 8tf)	〃	1,650	140
	⑨	Armor Stone (More than 1tf)	〃	840	160

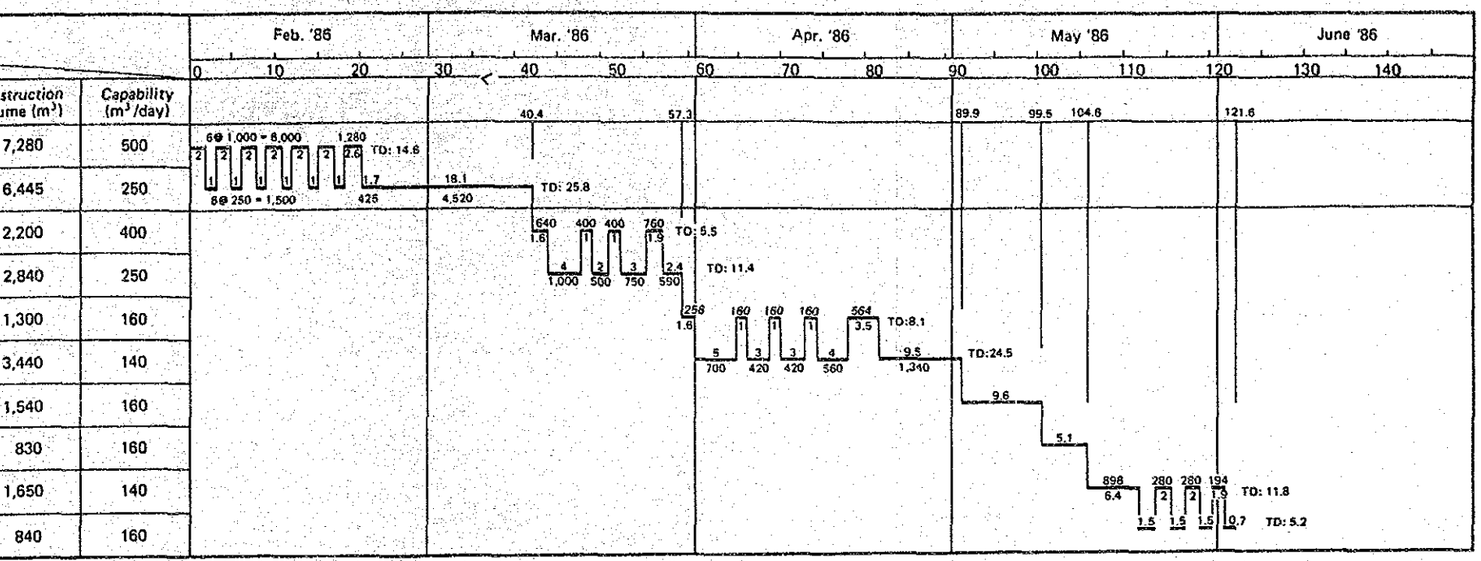

Notes:
1) T.D. shows the total days
2) m^3/D shows the production volume per day
3) The capability of stone placement of each construction step is estimated based on the field survey of the Study Team

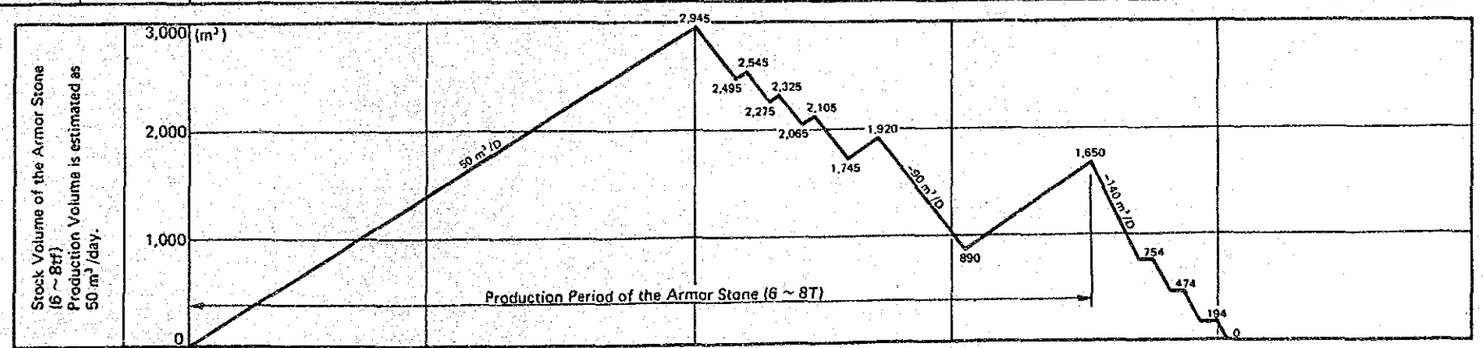

APPENDIX 5 DETAILS OF THE SIMULATION METHOD USING THE MATHEMATICAL MODEL "ONE-LINE THEORY"

1. General

1. 1 Outline of the Model

One-line theory is one of the methods used to estimate future shoreline changes caused by the littoral drift. The conception is shown in Fig. M-1.

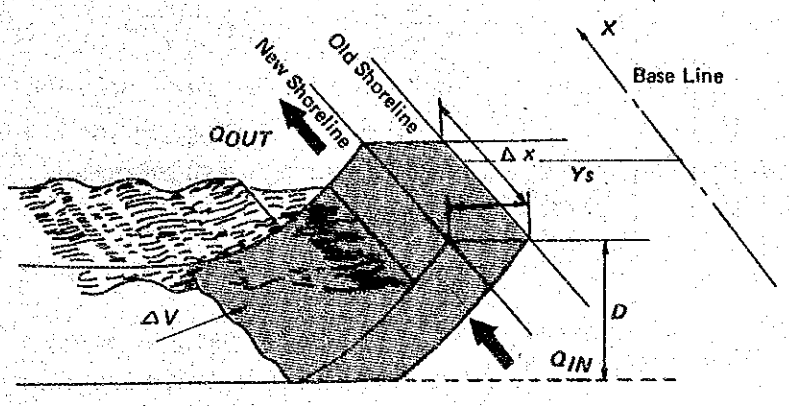

Fig. M-1 The Conception of the Shoreline Change

In this figure, the littoral drift sand volume at one end is Q_{IN}, and that at the other end is Q_{OUT}. The difference of the littoral drift sand volume ΔV equals $Q_{OUT}-Q_{IN}$. If Q_{OUT} is less than Q_{IN}, then the remaining drift sand is left in the divided mesh, and therefore, the shoreline advances. On the other hand, when Q_{OUT} is more than Q_{IN}, then ΔV becomes negative, and therefore, the shoreline recedes. The shoreline change Δy can be calculated using the following relation.

$$\Delta V = D \cdot \Delta x \cdot \Delta y \quad \cdots\cdots(1)$$

D is the depth of the sand drift zone.

This numerical model consists of two parts. The first is for the calculation of the wave deformation, and the second is for the calculation of the local littoral drift sand volume changes and the consequent shoreline changes.

1. 2 Calculation of Wave Deformation

(1) Deep water region

Wave deformation in the large area is calculated using the energy equilibrium equation as follows.

$$\frac{\partial D}{\partial t}+\nabla\ (D\vec{V})-Q=0 \quad \cdots\cdots(2)$$

in which,

$$\nabla=\left\{\frac{\partial}{\partial x},\ \frac{\partial}{\partial y},\ \frac{\partial}{\partial f},\ \frac{\partial}{\partial \theta}\right\} \quad \cdots\cdots(3)$$

$$\vec{V}=\begin{Bmatrix} V_x \\ V_y \\ V_f \\ V_\theta \end{Bmatrix}=\begin{Bmatrix} C_s\cos\theta \\ C_s\sin\theta \\ \dfrac{\partial f}{\partial t} \\ \dfrac{C_g}{C}\left(\dfrac{\partial C}{\partial x}\sin\theta+\dfrac{\partial C}{\partial y}\cos\theta\right) \end{Bmatrix} \quad \cdots\cdots(4)$$

C_g : Wave group velocity $\left\{=\dfrac{C}{2}\left(+\dfrac{2kh}{\sinh 2kh}\right)\right\}$ $\cdots\cdots(5)$

C : Celerity

k : Wave number

h : Water depth

Q : The net rate of energy added

The equations presented above are solved using the finite difference method under the conditions below.

(a) Deep water is assumed to be in a steady state

(b) The period of component waves does not change

(c) Q is assumed to be zero

(2) Shallow water region

The wave refraction, diffraction and shoaling are calculated independently and superposed as in Eq. (6). The wave refraction factor (K_r) is obtained solving Eq. (7)~Eg. (10).

$$H=K_r\cdot K_d\cdot K_s\cdot H_0 \quad \cdots\cdots(6)$$

$$\frac{D^2\beta}{Dt^2}+p\cdot\frac{D\beta}{Dt}+q\cdot\beta=0 \quad \cdots\cdots(7)$$

$$p=-2\left(\frac{\partial C}{\partial x}\cos\alpha+\frac{\partial C}{\partial y}\sin\alpha\right) \quad \cdots\cdots(8)$$

$$q=C\left(\frac{\partial^2 C}{\partial x^2}\sin^2\alpha-2\frac{\partial^2 C}{\partial x\cdot\partial y}\sin\alpha\cos\alpha+\frac{\partial^2 C}{\partial y^2}\cos^2\alpha\right) \quad \cdots\cdots(9)$$

$$K_r=(\beta)^{-1/2} \quad \cdots\cdots(10)$$

And the wave direction is obtained from Eq. (11),

$$\frac{D\alpha}{Dt} = \sin\alpha \frac{\partial C}{\partial x} - \cos\alpha \frac{\partial C}{\partial y} \quad \cdots\cdots(11)$$

Where C represents the wave velocity, t is time, α is the angle from the X-axis and H_0 is the wave height in deep water.

The diffraction factor (K_d) is obtained by Mitsui's method which uses the first term of the asympototic expansion of the Sommerfeld resolution of the Helmholtz equation. The shoaling factor (K_s) is obtained by Eq. (12) and Eq. (13),

$$K_s = \sqrt{\frac{C_0}{2nC}} \quad \cdots\cdots(12)$$

$$n = \frac{1}{2}\left(1 + \frac{4\pi h/L}{\sinh(4\pi h/L)}\right) \quad \cdots\cdots(13)$$

Where C represents the wave velocity, h is the water depth, L is the wave length, and C_0 is the wave velocity in deep water.

The initial line of breaking is determined by Eq. (14), which was proposed by Goda,

$$\frac{H_b}{L_0} = A\left\{1 - \exp\left[-1.5\frac{\pi h_b}{L_0}(1 + 15\tan^{4/3}\theta)\right]\right\} \quad \cdots\cdots(14)$$

Where H_b is the breaking wave height, L_0 is the wave length in deep water, h_b is the breaking water depth, $\tan\theta$ is a gradient of the seabed, and A is a constant (0.12~0.18).

The breaking energy flux is calculated by Eg. (15). Energy fluxes of diffracted waves coming from differernt directions are added as vectors.

$$F_b = \frac{1}{8}\rho g H_b^2 C_g \quad \cdots\cdots(15)$$

Where ρ is the density of sea water, g is the acceleration due to gravity, and C_g is the group velocity of the waves.

1. 3 Calculation of Shoreline Changes

Two equations are necessary to calculate the shoreline change. One is Eq. (16) which is for the continuity of sand transport in the alongshore direction,

$$\frac{\partial y}{\partial t} + \frac{1}{h} \cdot \frac{\partial Q_1}{\partial x} = 0 \quad \cdots\cdots(16)$$

Where h is the vertical range of the profile change, y is the shoreline location, and Q_1 is the volume of littoral sand drift.

The other is Eq. (17) which is for alongshore sediment transport,

$$Q_1 = \frac{\xi}{\gamma_s}(EC_g)\, b\, (\sin 2\alpha_b - 3.24\frac{\partial H_b}{\partial x}\cot\beta\, \cos\alpha_b) \quad \cdots\cdots(17)$$

Where $(EC_g) \cdot b$ is the breaking wave energy flux, ξ is a constant and α_b is the angle the wave crest makes with the shoreline when breaking. γ_s is the density of beach material in place, and β is the slope of the beach.

2. Calculation Conditions

2. 1 Wave Conditions

Based on the observed wave date described in CHAPTER IV, the wave period is calculated by Eq. (18).

$$T_n = \sum_{i=1}^{N} T_i / N \quad \cdots\cdots (18)$$

Where T_n is the representative wave period for the calculation, T_i is the wave period of each observation, and N is the total number of observation data.

The representative wave height (H_n) is calculated using Eq. (19), so that $H_n^2 \times C_{gn}$ equals the total amount of the wave energy fluxes.

$$(\sum_{i=1}^{N} H_i^2 \ C_{gi}) / N = H_n^2 \ C_{gn} \quad \cdots\cdots (19)$$

Where H_i is the height of each observation, C_{gi} is the group velocity of each wave, and C_{gn} is the group velocity corresponding to the representative wave period T_n. The calculation results of the representative wave conditions are as follows :

$H_n = 1.0$ m
$T_n = 12.0$ s
Wave Direction N 210° (S 30°W)
S_{max} (directional spreading parameter) = 75

2. 2 Tidal Condition

The tidal condition for the calculation is as follows :

M.S.L. = D.L. + 1.40 m

2. 3 The Grain Size for the Calculation

A median diameter of 0.3 mm is used for the calculation.

2. 4 The Depth of the Sand Drift Zone

The depth of the sand drift zone is decided from the wave up-rush height and the critical water depth for sediment movement. The result is as follows :

Wave Up-rush Height	3.2 m (above D.L. + 1.40 m)
Critical Water Depth for Sediment Movement	5.4 m (below D.L. + 1.40 m)
Depth of Sand Drift Zone, (D)	8.6 m

There is some modification of the above D value in the process of the calculation.

2. 5 Alternative Breakwater Extension Lengths

The length of the alternative breakwater extension plans are shown in Fig. M—2.

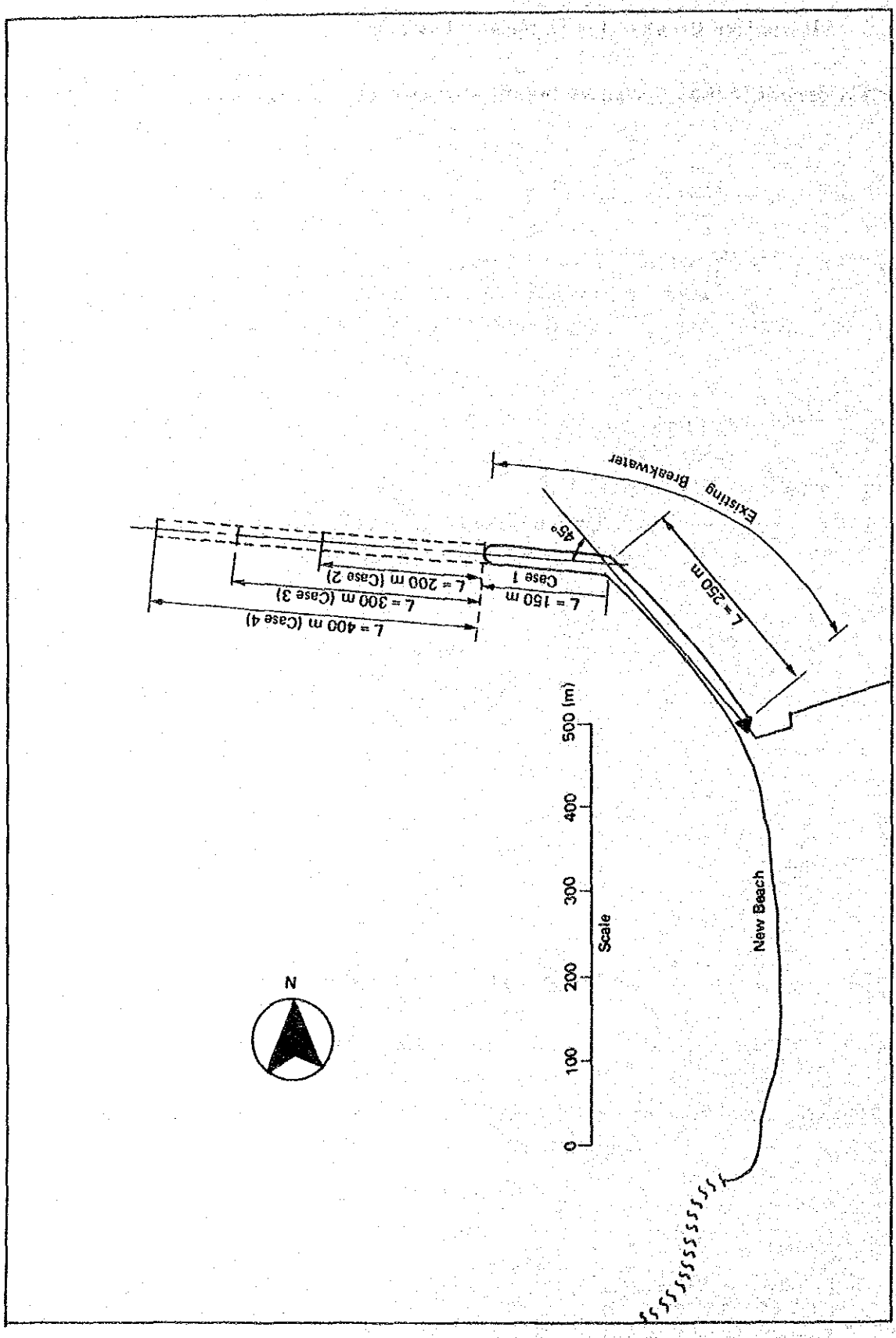

Fig. M-2 Alternative Designs of the Breakwater Extension

APPENDIX 6 DETAILS OF THE SIMULATION METHOD USING THE MATHEMATICAL MODEL: "DEPTH MODEL"

The depth model consits of 4 calculation programs. They are :

(1) Tidal Current Simulation Program
(2) Longshore Current Simulation Program
(3) Wave Deformation Calculation Program
(4) Sand Transport Simulation Program

The flow chart of these programs is shown in Fig. M—1.

1. Current Simulation Model

The governing equations consist of the continuity equation and the equations of motions as shown below.

$$\frac{\partial \zeta}{\partial t}+\frac{\partial}{\partial x}\left[(\zeta+h)\ u\right]+\frac{\partial}{\partial y}\left[(\zeta+h)\ v\right] \quad \cdots\cdots(1)$$

$$\frac{\partial u}{\partial t}+u\frac{\partial u}{\partial x}+v\frac{\partial u}{\partial y}=-fv-g\frac{\partial \zeta}{\partial x}+A_x\frac{\partial^2 u}{\partial x^2}+A_y\frac{\partial^2 u}{\partial y^2}-\gamma_b^2\frac{u(u^2+v^2)^{1/2}}{(\zeta+h)} \quad \cdots(2)$$

$$\frac{\partial v}{\partial t}+u\frac{\partial v}{\partial x}+v\frac{\partial v}{\partial y}=-fu-g\frac{\partial \zeta}{\partial y}+A_x\frac{\partial^2 v}{\partial x^2}+A_y\frac{\partial^2 v}{\partial y^2}-\gamma_b^2\frac{v(u^2+v^2)^{1/2}}{(\zeta+h)} \quad \cdots(3)$$

where u, v: component of the mean horizontal velocity in the x, y direction, respectively
ζ: free surface displacement
h: water depth
t: time
f: coriolis parameter
g: gravitational acceleration
γ_b^2: bottom friction coefficient
A_x, A_y: lateral mixing coefficient

2. Longshore Current Simulation Model

In the model, mostly wave induced currents are considered. The following equations including radiation stress terms due to waves are used to calculate the current distribution.

$$\frac{\partial \zeta}{\partial t}+\frac{\partial}{\partial x}\left\{u\ (\zeta+h)\right\}+\frac{\partial}{\partial y}\left\{v\ (\zeta+h)\right\} \quad \cdots\cdots(4)$$

$$\frac{\partial u}{\partial t}+u\frac{\partial u}{\partial x}+v\frac{\partial u}{\partial y}+g\frac{\partial \zeta}{\partial x}+\frac{F_x}{(\zeta+h)}-A_l\left(\frac{\partial^2 u}{\partial x^2}+\frac{\partial^2 u}{\partial y^2}\right)+R_x=0 \quad \cdots\cdots(5)$$

$$\frac{\partial v}{\partial t}+u\frac{\partial v}{\partial x}+v\frac{\partial v}{\partial y}+g\frac{\partial \zeta}{\partial y}+\frac{F_y}{(\zeta+h)}-A_l\left(\frac{\partial^2 v}{\partial x^2}+\frac{\partial^2 v}{\partial y^2}\right)+R_y=0 \quad \cdots\cdots(6)$$

where u, v: component of the mean horizontal velocity

in the x, y direction, respectively

ζ: mean free surface displacement

F_x, F_y: bottom friction terms in the x, y direction, respectively

A_l: lateral mixing coefficient

R_x, R_y: radiation stress terms in the x, y direction, respectively

3. Sand Transport Simulation Model

In this study, Bijker's Formula is used to estimate the sand sedimentation in the harbour basin. The influence of currents and waves is considered through the introduction of an increased bed shear and a subsequently higher diffusion coefficient. The sedimentation process and the estimation method are outlined as follows.

The vertical distribution of the suspended sediment is described by the following basic equation.

$$WC+\varepsilon\frac{dC}{dz}=0 \quad \cdots\cdots(7)$$

where W: fall velocity of the sediment in still water

C: concentration at height z above the bed

ε: diffusion coefficient for the suspended material at height z

The sedimentation process is shown in Fig. M—2. The total suspended load at section ① is expressed by :

$$S_{s1}= C_1 \cdot V_1 \cdot h_1 \quad \cdots\cdots(8)$$

Immediately after the change of depth from h_1 to h_2, that is in section ②, the value of $\bar{C}$ will remain constant. However, the vertical gradient of the sediment concentration will decrease by a factor h_1/h_2 and sedimentation $S_v(0)$ will occur due to the velocity decrease. At the voluntary section x, the sediment $S_v(x)$ will be found under the condition of $\bar{C}_2(x)$ and this situation will continue to section ③. If the channel width is large enough, the concentration will be settled and no sediment will occur in section ④.

In practice, the sedimentation in the channel is limited to $S_v = \int_0^B S_v(x)$.

Since the actual sedimentation, or vertical transport is determined by the condition just above the bed, the sedimentation is expressed by :

$$S_v= WC_{b2} + \varepsilon\,(dc/dz)_b \quad \cdots\cdots(9)$$

in which the subscript b indicates the situation at the bed.

Where, $\varepsilon= 0.18\ V_*\ h$

$$C= C_b \exp(-wz/\varepsilon) \quad \cdots\cdots(10)$$

$$\bar{C}= (C_b \cdot \varepsilon/wh)\ \{1-\exp(-wh/\varepsilon)\} \quad \cdots\cdots(11)$$

The wave and current effects are taken into account through an increased bed shear.

$$V_{*cw} = V_{*c} \{1 + 1/2 (\xi u/\bar{V})^2\} \quad \cdots\cdots(12)$$

in which V_{*cw} and V_{*c} are the bed shear velocities due to wave and current.

$$\xi = C (f_w/29)^{1/2} \quad \cdots\cdots(13)$$

Where, f_w : friction coefficient by Jonsson

u : amplitude of the horizontal orbital velocity at the bed

From equation (9)

$$S_v(0) = WC_{b2} \left(1+\frac{h_1 \varepsilon_2}{h_2 \varepsilon_1}\right) \quad \cdots\cdots(14)$$

The vertical transport S_v is expressed in m^2/s per unit of bed surface.

If we assume that $S_s(x)$ decreases exponentially with x,

$$S_s(x) = f (\exp (-\beta x)) \quad \cdots\cdots(15)$$

With the boundary conditions shown in Fig. M—2, equation (9) can be written as :

$$S_v(x) = \beta(\beta s_1 - \beta s_2)\exp (-\beta x) \quad \cdots\cdots(16)$$

These equations make it possible to compute in a quick and simple manner the sedimentation in the channels.

4. Divided Area in Caldera Bay

The trend of the water depth change from August 1982 to September 1985 is calculated based on the sounding results of Caldera Bay. The calculation area is divided into 9 as shown in Fig. M—3.

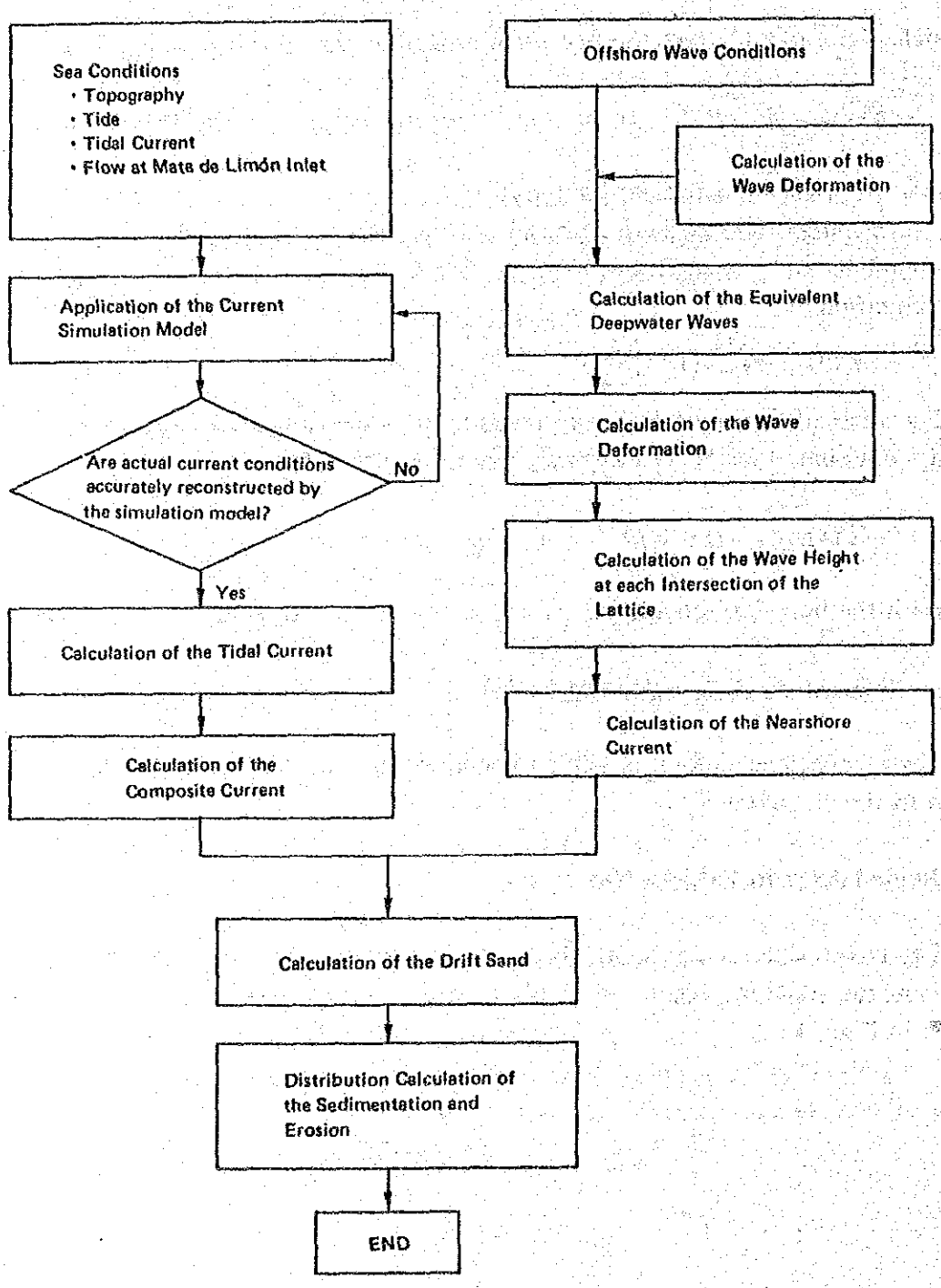

Fig. M-1 Calculation Procedure of the Depth Change Using the Simulation Model

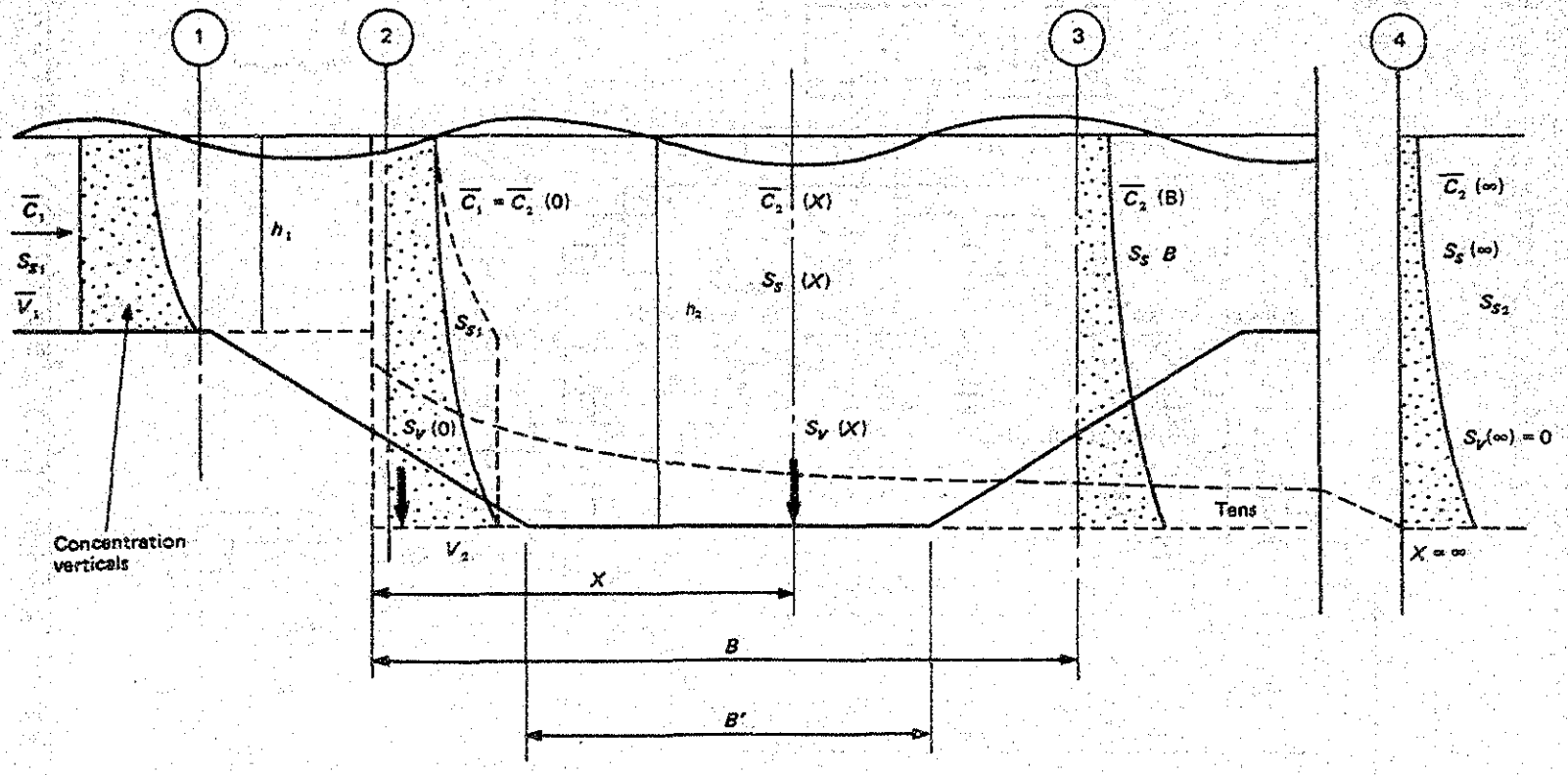

Fig. M-2 Mechanism of Sedimentation

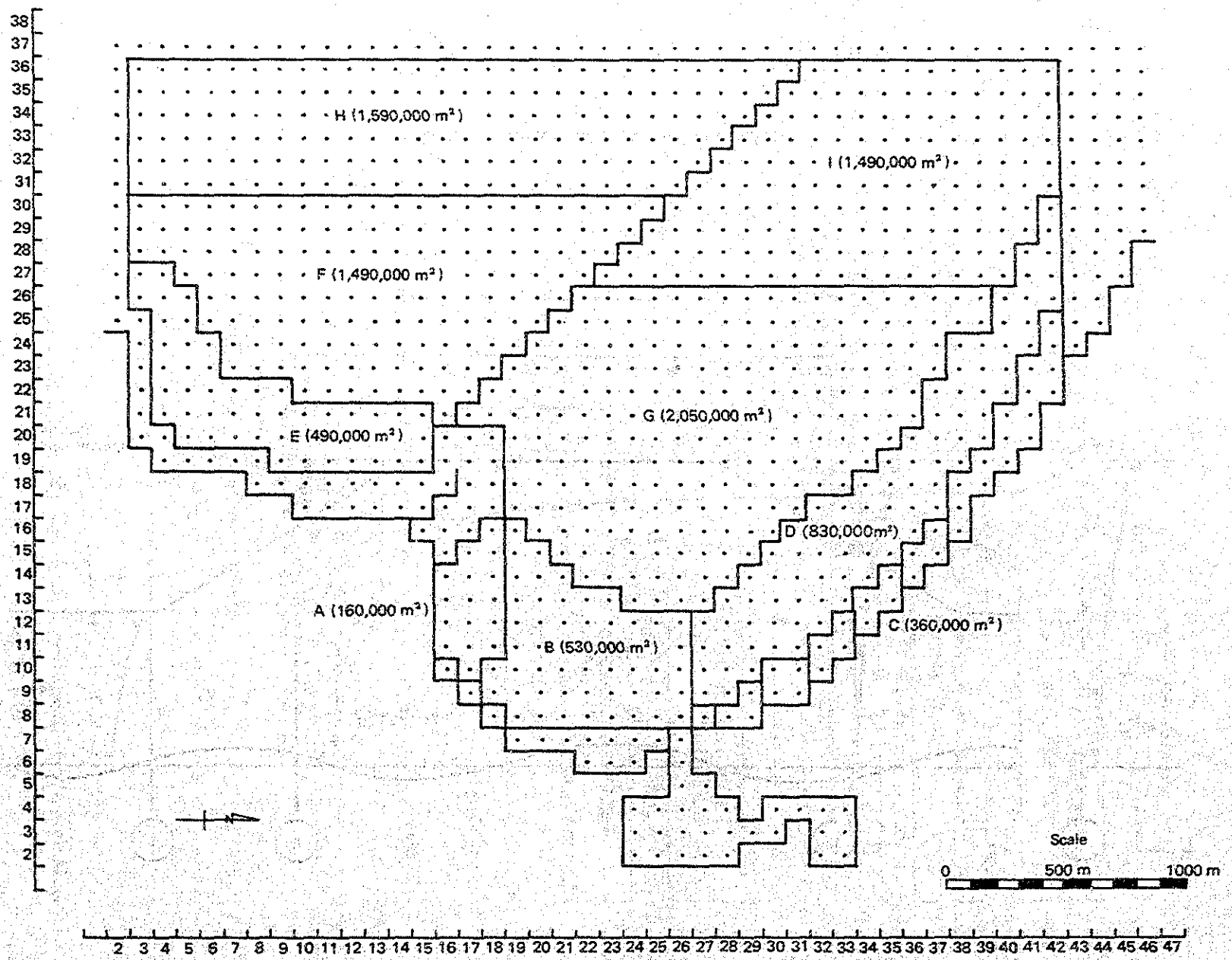

Fig. M-3 Divided 9 Areas in Caldera Bay

APPENDIX 7 PROJECTED SOCIOECONOMIC FRAME

The major projected national socioeconomic indices, that is population and GDP, are listed in Table M−1 and M−2, respectively.

Table M-1 Projected Population

Year	Population (persons)	Compound increase rate (%)
1982	2,371,519	2.78
1983	2,434,601	2.66
1984	2,498,145	2.61
1985	2,569,597	2.58
1986	2,628,199	2.56
1987	2,694,693	2.53
1988	2,761,790	2.49
1989	2,828,902	2.43
1990	2,895,381	2.35
1991	2,961,685	2.29
1992	3,027,731	2.23
1993	3,093,735	2.18
1994	3,159,323	2.12
1995	3,224,405	2.06
1996	3,289,215	2.01
1997	3,353,355	1.95
1998	3,417,404	1.91
1999	3,481,309	1.87
2000	3,545,017	1.83

Table M-2 Projected GDP

Year	GDP at 1966 constant prices (Unit : million colones)
1983	8,947.7
1984	9,513.0
1985	9,426.2
1986	9,540.9
1987	9,750.8
1988	10,014.1
1989	10,274.4
1990	10,521.0
1991	10,784.0
1992	11,053.6
1993	11,330.0
1994	11,613.2
1995	11,903.5
1996	12,201.1
1997	12,506.2
1998	12,818.8
1999	13,139.3
2000	13,467.8